AD-A087 109 IOWA UNIV IOWA CITY DEPT OF PHYSICS AND ASTRONOMY F/G 3/2
SOURCES AND SINKS OF ENERGETIC ELECTRONS AND PROTONS IN SATURN'--ETC(U)
APR 80 J A VAN ALLEN, B A RANDALL N00014-76-C-0016
UNCLASSIFIED U. OF IOWA-80-16 NL

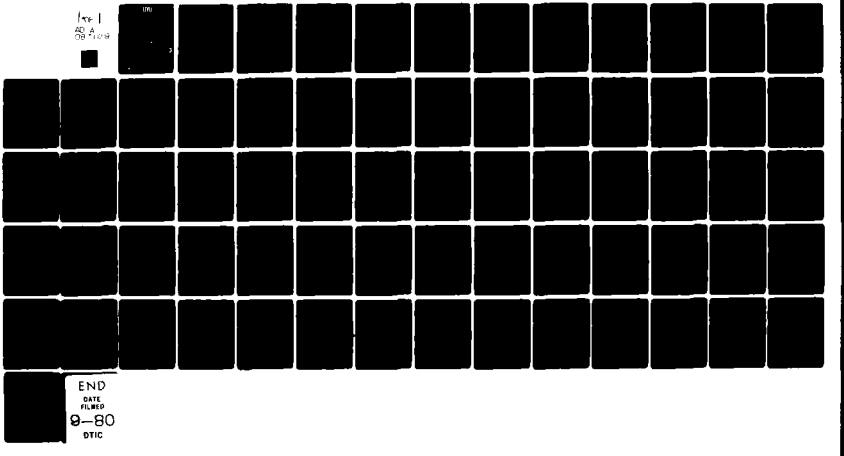

END
DATE FILMED
9-80
DTIC

LEVEL II

12 SC

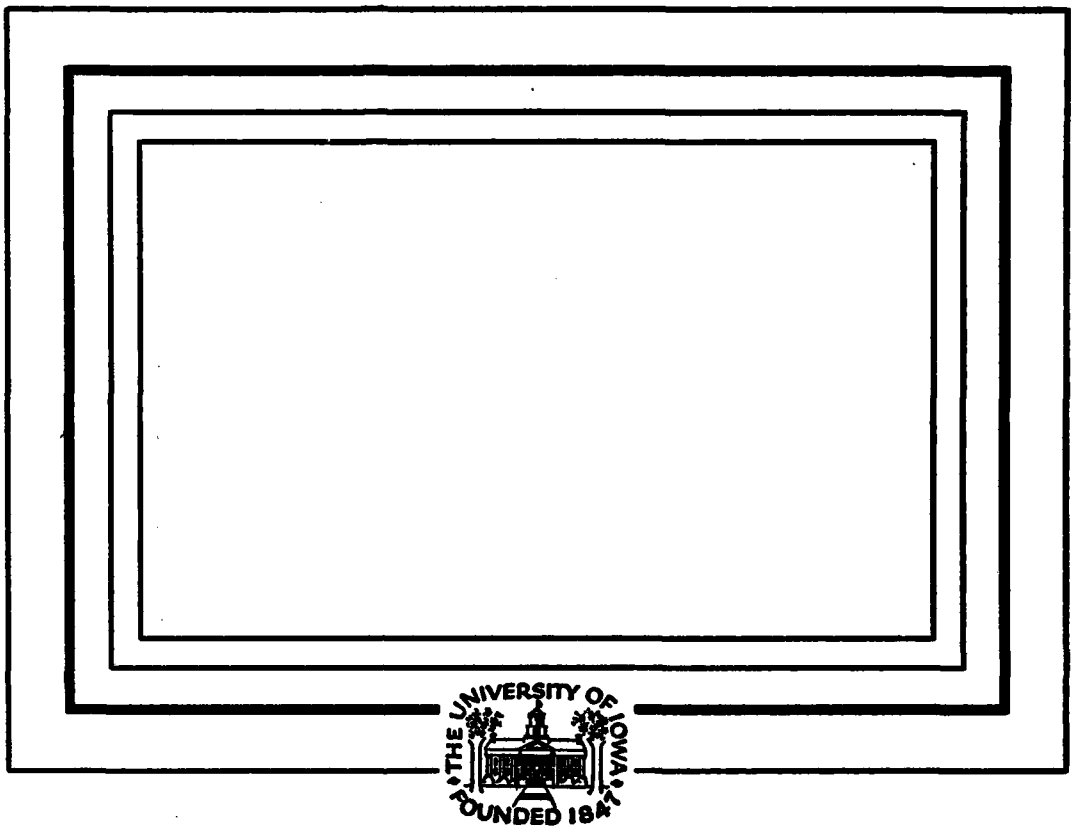

Department of Physics and Astronomy

THE UNIVERSITY OF IOWA

Iowa City, Iowa 52242

80 7 23 00

U. of Iowa 80-16

12

Sources and Sinks of Energetic Electrons and Protons in Saturn's Magnetosphere

by

J. A. VAN ALLEN, B. A. RANDALL,
and M. F. THOMSEN

Department of Physics and Astronomy
The University of Iowa
Iowa City, Iowa 52242

June 1980

Revised version of original manuscript of 1 May 1980.

In press, J. Geophys. Res.

UNCLASSIFIED

SECURITY CLASSIFICATION OF THIS PAGE (When Data Entered)

REPORT DOCUMENTATION PAGE	READ INSTRUCTIONS BEFORE COMPLETING FORM
1. REPORT NUMBER (14) U. of Iowa-80-16	2. GOVT ACCESSION NO. AD-A087 409
	3. RECIPIENT'S CATALOG NUMBER --
4. TITLE (and Subtitle) (6) SOURCES AND SINKS OF ENERGETIC ELECTRONS AND PROTONS IN SATURN'S MAGNETOSPHERE.	5. TYPE OF REPORT & PERIOD COVERED Progress, April 1980
	6. PERFORMING ORG. REPORT NUMBER --
7. AUTHOR(s) (10) J. A. Van Allen, B. A. Randall, and M. F. Thomsen	8. CONTRACT OR GRANT NUMBER(s) (15) N00014-76-C-0016
9. PERFORMING ORGANIZATION NAME AND ADDRESS Department of Physics and Astronomy The University of Iowa Iowa City, Iowa 52242 (9) Progress Rept.	10. PROGRAM ELEMENT, PROJECT, TASK AREA & WORK UNIT NUMBERS --
11. CONTROLLING OFFICE NAME AND ADDRESS Office of Naval Research Electronics Program Office Arlington, Virginia 22217	12. REPORT DATE (11) April 1980
	13. NUMBER OF PAGES 63
14. MONITORING AGENCY NAME & ADDRESS(if different from Controlling Office) (12) 74	15. SECURITY CLASS. (of this report) UNCLASSIFIED
	15a. DECLASSIFICATION/DOWNGRADING SCHEDULE

16. DISTRIBUTION STATEMENT (of this Report)

Approved for public release; distribution is unlimited.

17. DISTRIBUTION STATEMENT (of the abstract entered in Block 20, if different from Report)

18. SUPPLEMENTARY NOTES

To be published in Journal of Geophysical Research.

19. KEY WORDS (Continue on reverse side if necessary and identify by block number)

SATURN
SATURN'S MAGNETOSPHERE
PLANETARY MAGNETOSPHERES

20. ABSTRACT (Continue on reverse side if necessary and identify by block number)

[See page following.]

188 460

DD FORM 1 JAN 73 1473 EDITION OF 1 NOV 65 IS OBSOLETE
S/N 0102-LF-014-6601

UNCLASSIFIED
SECURITY CLASSIFICATION OF THIS PAGE (When Data Entered)

ABSTRACT

This paper reports the results of continuing analysis and interpretation of energetic particle observations obtained by the University of Iowa instrument on Pioneer 11 during traversal of Saturn's magnetosphere in August-September 1979. On the basis of the radial dependence of the phase space density of very energetic protons ($E_p > 80$ MeV) and estimates of the necessary source strength, it is reasonably certain that cosmic ray neutron albedo from the planet's atmosphere and Rings A and B is the source of such particles. At radial distance $r = 2.7\ R_S$ and for $E_p > 80$ MeV, the ratio of source strength S to radial diffusion coefficient D is $2 \times 10^{-24}\ cm^{-5}$. A reasonable pair of values is $S \sim 7 \times 10^{-15}\ cm^{-3}\ s^{-1}$ and $D \sim 1 \times 10^{-10}\ R_S^2\ s^{-1}$. The spectrum of electrons $0.040 < E_e <$ (a few MeV) and the radial dependence of the phase space density of such electrons are derived. The source of these electrons is at the magnetosheath. The source of protons $E_p \sim 1$ MeV is also at the magnetosheath and may be either thermalized solar wind or energetic interplanetary protons which were unusually abundant at the time of Pioneer 11's encounter. Low energy electrons and protons experience strong losses inward of $r \sim 10\ R_S$,

apparently attributable to the large inner satellites Rhea, Dione, Tethys, Enceladus, and Mimas and to a broad tenuous ring of particulate matter (Ring E) and/or gas. There were important temporal changes in the distributions of low energy electrons and protons within a period of ~ 10 hours between inbound and outbound passes, probably caused by unusually disturbed interplanetary conditions.

INTRODUCTION

Discovery of the magnetosphere of Saturn and many detailed features thereof have been reported in earlier papers [Wolfe et al., 1980; Smith et al., 1980; Simpson et al., 1980; Van Allen et al., 1980; Trainor et al., 1980; Fillius et al., 1980; and Acuna and Ness, 1980].

Further analysis of the University of Iowa observations of energetic particles [Van Allen et al., 1980] [Paper I] during Pioneer 11's August-September 1979 encounter with Saturn is presented in this paper. Progress has been made on identifying particle species, on determining energy spectra, and on delineating the sources and sinks of energetic electrons and protons.

Principal features of the encounter trajectory, given in Figures 1 and 2 and Table 1, have been derived from post-encounter data supplied to investigators by the Ames Research Center of the National Aeronautics and Space Administration, the agency responsible for the Pioneer 11 spacecraft and mission.

Note that all distances herein are given in units of the adopted equatorial radius of Saturn (1 R_S = 60,000 km) and all times are Earth Received Time (ERT) in Universal Time (UT) of reception of the telemetry signal at the earth (Table 1).

Because of the nearly equatorial nature of the encounter trajectory (Figure 2) and the nearly centered, untilted, dipolar nature of the planet's inner magnetic field [Smith et al., 1980; Acuna and Ness, 1980], there is a trivial distinction between a radial distance r and the corresponding magnetic shell parameter L for $r \leq 6$.

A general overview of our observations of energetic charged particles in Saturn's magnetosphere was given in Figure 1 of Paper I and is reproduced here for convenient reference as Figure 3. The principal characteristics of the various detectors in our instrument are summarized in Table 2. A thorough discussion of individual detectors and of our procedure for the identification of particle species is given in Appendices A and B.

SOURCES AND SINKS OF HIGH ENERGY PROTONS ($E_p > 80$ MeV)

The basic problem of planetary magnetospheric physics is the determination of the physical causes of observed particle distributions [Hess, 1968; Roederer, 1970; Schulz and Lanzerotti, 1974]. It is supposed that there are sources and sinks of particles and that particles diffuse inward and outward in response to time variable electric and magnetic fields or magnetic flux tube interchange, conserving the first and second adiabatic invariants, μ and J, but violating the third, Φ. There is at least one firmly known boundary condition in such problems, namely a perfect absorber at the top of the appreciable atmosphere of the planet or, in the case of Saturn, at the outer edge of Ring A [Paper I]. The usual technique is to work with the diffusion equation for a dipolar magnetic field:

$$\frac{\partial f}{\partial t} = L^2 \frac{\partial}{\partial L} \left(\frac{D}{L^2} \frac{\partial f}{\partial L}\right) + \mathcal{S} - \mathcal{L} . \qquad (1)$$

In equation (1), f is the phase space density of a given species of particle at constant μ and constant J, L is the McIlwain magnetic shell parameter, $\mathcal{S}$ is the source strength, $\mathcal{L}$ is the sink strength,

and D is the radial diffusion coefficient in phase space. In general, D is a function of L; it is often approximated by a power law dependence $D_o L^n$ with the index n independent of L.

Case I

If (a) $\mathcal{S} = \mathcal{L} = 0$ throughout the interior of the magnetosphere; (b) there is a perfect absorber (sink) at the inner boundary L_o; (c) the only source of particles is at the outer boundary (the magnetosheath); and (d) ∂(any quantity)/$\partial t = 0$ (time stationary state), then from (1)

$$\frac{D}{L^2} \frac{\partial f}{\partial L} = \text{const.} \qquad (2)$$

The constant in (2) must be positive because D, L, and f are intrinsically positive quantities and $\partial f/\partial L$ is positive at the inner boundary. Hence the phase space density f must decline monotonically from its value at the outer boundary to zero at the inner boundary; i.e., there can be no maxima or minima in f(L) regardless of the form of D(L).

Case II

If conditions are the same as for Case I except that the sink strength $\mathcal{L}$ (an intrinsically positive quantity) is not zero on either a localized or distributed basis, then from (1)

$$\frac{D}{L^2} \frac{\partial f}{\partial L} = \int_{L_o}^{L} \frac{\mathcal{L}}{L^2} \, dL \, . \qquad (3)$$

The integral in (3) is positive and again it is seen that there can be no maxima or minima in f(L).

Case III

If the conditions are the same as for Case II except that $\mathcal{S} \neq 0$ (i.e., internal sources exist), then it is possible for $\partial f/\partial L$ to change algebraic sign between L_o and the outer boundary and maxima and minima in f(L) can occur, even in a time stationary state.

Case IV

It is possible for an absorber of particles (e.g., a satellite), localized in L and in longitude, to produce a minimum in f(L) over a restricted range of longitude [Paper I] but a minimum can not be present in the longitudinally averaged value of f(L) unless there are sources at both lesser and greater values of L. In this example $\partial f/\partial t$ is not zero everywhere though it may be approximately so overall.

As a practical remark on the foregoing considerations it may be noted that, in the case of sufficiently steep particle spectra, it is possible to have a minimum in particle intensity j(L) at constant energy even though f(L) at constant μ and J has no minimum.

The proper computation of f(L) at any selected pair of constant values of μ and J from observed data requires an extensive knowledge of the absolute differential energy spectrum of the particles as a function of pitch angle throughout the

magnetosphere. Such a requirement far exceeds the omnidirectional intensity above a single proton energy (80 MeV) that we have available from our detectors C and D [Appendix B]. We have adopted a simplified basis for the computation of f(L) by (a) ignoring the (unknown) L-dependence of the pitch angle distribution (which usually has a rather weak influence on the results); (b) assuming that the spectral form over the relevant range of energy E is of the form $j \propto E_p^{-\gamma}$ with γ = constant; and (c) taking the observed omnidirectional intensity (counting rate of detector C) to represent the integral unidirectional intensity of protons ($E_p > 80$ MeV) at pitch angle $\alpha = 90°$ (i.e., J = 0). A sample result of such calculations using observed values of the magnetic field strength [Smith et al., 1980] is shown in Figure 4 for $\gamma = 1.3$. The qualitative nature of the dependence of f on r (= L) is quite insensitive to γ. The adopted value of $\mu = 8.317 \times 10^3$ MeV/gauss is such that the range of the corresponding values of E_p is from 24 MeV at r = 4.1 to 128 MeV at r = 2.3, thus spanning our instrumental threshold of 80 MeV. f(r) would have essentially zero values at Mimas and at Ring G if the contribution of electron bremsstrahlung to the rate of detector C had been subtracted [Appendix B]. The principal features of Figure 4 are that there are three maxima in f(r) -- at r = 3.37, 2.68, and 2.42 -- separated by null values at Mimas' orbit and at Ring G and bounded by null values at Ring F on the inward end and for

$r \geq 4.1$ on the outward end. These principal features are robustly independent of approximations in our simplified treatment. Essentially identical curves are obtained for both inbound and outbound data, suggesting a time-stationary situation despite very disturbed interplanetary conditions during the encounter.

We consider that Figure 4 provides unequivocal evidence (Case III above) for an internal source of the high energy protons in Saturn's magnetosphere. Further conclusions are(a) that Mimas and Rings G and F serve as effective absorbers of such particles and (b) that there are either losses or a markedly reduced source strength and/or a markedly increased value of D for $r \geq 4.1$. There is also persuasive evidence for partial absorption by our previously suspected satellite 1979 S3 at $r = 2.84$ [Paper I]. The entire curve of $f(r)$ is totally incompatible with an external source, e.g., the magnetosheath; moreover such a source would need to supply protons of energies of the order of 0.3 MeV at the magnetopause, a value at least 100 times greater than could reasonably be expected for thermalized solar wind particles (though possibly available during solar energetic particle events). The leading candidate source of the high energy protons is cosmic ray neutron albedo (Crand), suggested most forcefully for Saturn's magnetosphere by Fillius et al. [1980]. (The value of γ in Figure 4 is a retrospective choice from a family of different trial computations and is based on the spectrum of high energy protons in the earth's inner radiation belt [Hess, 1968].) Indeed we are unable to suggest

a physically plausible alternative. A full quantitative estimate of the expected source strength of Crand at Saturn has not yet been made but the following discussion examines the matter in a preliminary way.

Mimas and Ring G are taken to be perfect absorbers and $\mathcal{S}$ denotes the source strength of injected protons from the decay of albedo neutrons from the atmosphere of the planet and from its rings. The essence of the problem is illustrated by a simple time-stationary solution of the one-dimensional diffusion equation in configuration space, with constant $\mathcal{S}$ and constant D over a small range of L.

$$D \frac{\partial^2 N}{\partial x^2} = -\mathcal{S}. \qquad (4)$$

In equation (4), N is the number density of protons and $\mathcal{S}$ is the source strength (the number of injected protons per unit volume per unit time) and x is effectively the radial coordinate.

The solution of equation (4) subject to the boundary conditions N = 0 and x = -a and at x = +a is

$$N = \frac{\mathcal{S}}{2D} (a^2 - x^2), \qquad (5)$$

a curve resembling any one of the three peaks in Figure 4. By (5), the maximum value N_{max} ($= \mathcal{S}\, a^2/2D$) occurs at x = 0, halfway between the absorbing boundaries. Starting with N = 0 throughout the region, the time T required to build up the equilibrium situation is of the order of $N_{max}/\mathcal{S} = a^2/2D$.

For the major peak at r = 2.68 in Figure 4, $N_{max} \sim 2.6 \times 10^4/0.4\ c = 2.2 \times 10^{-8}$ cm^{-3} ($E_p > 80$ MeV) and $a \sim 1.5 \times 10^9$ cm. Hence,

$$\frac{\mathcal{S}}{D} \sim 2 \times 10^{-24} \text{ cm}^{-5}, \qquad (6)$$

a value probably reliable to within a factor of 2. For representative values of D, the approximate absolute values of the source strength $\mathcal{S}$ and build-up T are as follows: For $D = 1 \times 10^{-10}$ R_S^2 s^{-1}, $\mathcal{S} \sim 7 \times 10^{-15}$ cm^{-3} s^{-1}, T ~ 10 yr; 1×10^{-9}, 7×10^{-14}, 1; and 1×10^{-8}, 7×10^{-13}, 0.1.

No detailed estimate of $\mathcal{S}$ from first principles has yet been made for Saturn. Indeed such estimates for the earth occupied the efforts of many persons for over a decade before a reasonably credible quantitative explanation of energetic proton intensities in the inner radiation belt was achieved [White, 1973].

Meanwhile, a crude comparison of $\mathcal{S}$ at Saturn and at the earth can be made along the following lines:

(a) If $I(\theta, \zeta, \psi)$, the directional intensity of albedo neutrons emitted upward per unit solid angle per unit area per unit time at colatitude θ, zenith angle ζ, and azimuth ψ (Figure 5), is identical for two spheres of radii a and a', then by geometric similitude the omnidirectional intensity at

external points P and P' at radial distances r and r' from the centers of the respective spheres is the same if $r/a = r'/a'$. Because the mean lifetime of a neutron at rest is 1013 seconds, the mean flight path of an energetic neutron is enormously greater than any distance with which we are concerned. Thus, since the probability of decay per unit distance is independent of radial distance, the source strength β is the same at P as it is at P'.

(b) The molecular compositions of the atmospheres of Saturn and the earth are quite different, the former being about 90 percent H_2 and 10 percent He [Orton and Ingersoll, 1980] and the latter 78 percent N_2 and 21 percent O_2. The production of neutrons of energy $\geq$ 50 MeV in nuclear reactions by energetic cosmic rays (E $\geq$ several GeV) is primarily a knock-on process. The essential target parameter is the number of neutrons in atmospheric gases in a column of length equal to an interaction length. On this basis and considering both proton and helium nuclei in the primary cosmic ray beam, we estimate that the rate of production of high energy neutrons in Saturn's upper atmosphere is about 0.4 of that in the earth's, if both are exposed to the same cosmic ray bombardment.

(c) Another significant difference between Saturn and the earth is the difference in their general magnetic fields. The vertical Stoermer momentum cutoff pc for a particle

of charge Ze at the surface of a planet of dipolar moment M and radius a is given as a function of magnetic colatitude θ by

$$pc = \frac{Ze\,M}{4a^2} \sin^4 \theta \qquad (7)$$

[Paper I; Sauer, 1980]. For the same value of pc,

$$\left(\frac{\sin \theta_S}{\sin \theta_E}\right)^4 = 0.17 \qquad (8)$$

where subscripts S and E denote Saturn and the earth, respectively. Some pairs of corresponding values of colatitude θ_E and θ_S are as follows: 90°, 40°; 60°, 34°; and 30°, 19°. Thus, it is clear that the effective fraction of Saturn's atmospheric surface for the emission of neutrons is about 0.4 of that of the earth's.

(d) On the basis of considerations (a), (b), and (c) it appears that $\not{\beta}$ at a given value of r/a in Saturn's magnetosphere would be about one-sixth of that at the same r/a in the earth's.

(e) However, a compensatory increase in $\not{\beta}$ at Saturn is provided by neutron production in the surfaces of Rings A and B [Fillius et al., 1980]. The surface areas (both sides) of Rings A and B exceed the entire surface area of the planet and the vertical (meridian plane) Stoermer cutoff in the ring plane

($\theta = 90°$) at $r = 2$ is equal to that on the planet's surface ($r = 1$) at $\theta = 45°$.

Our tentative conclusion is that β at a given position in Saturn's magnetosphere is of the same order of magnitude as that at the same scaled position in the earth's magnetosphere [White, 1973]. For injected protons of $E_p > 80$ MeV, β at $r = 2.7$ is $\sim 7 \times 10^{-16}$ cm^{-3} s^{-1} corresponding by equation (6) to a diffusion coefficient $D \sim 1 \times 10^{-10}$ R_s^2 s^{-1}, a plausible value.

Within the framework of the foregoing interpretation, it appears likely that there is an as-yet-unobserved belt of trapped energetic protons between the inner edge of Ring C and the planet.

SOURCES AND SINKS OF ELECTRONS ($0.040 < E_e <$ a few MeV)

As discussed in Appendix A, the counting rate differences (A - C) and (B - C) provide absolute values of the unidirectional intensity of electrons $E_e > 0.040$ and > 0.56 MeV, respectively.

As shown in Figure 3 and more fully in Figure 6, the counting rate of A rises precipitously just inside the magnetopause on the inbound leg of the trajectory. Thereafter it continues to rise monotonically to a local maximum at $r \sim 12$, then has a local minimum at 10.5, a second maximum at 7.5 and a second minimum at 5. For lesser values of r, $A \simeq B$, i.e., there are essentially no electrons in the spectral range 0.040 to 0.56 MeV. The counting rate of B rises monotonically and nearly exponentially from the magnetopause inward (Figure 7) to the outer edge of Ring A. The outbound rates have a similar dependence on r except that they decline much more gradually outside of $r \sim 12$ on the outbound leg of the trajectory (near local dawn) than they do on the inbound leg (near the noon meridian).

The observed counting rate ratio (A - C)/(B - C) vs r is shown by solid circles in Figure 8. If the unidirectional differential intensity $j \propto E_e^{-\gamma}$ down to values of $E_e < 0.040$ MeV,

$$\left(\frac{A - C}{B - C} \right) = (14)^{\gamma - 1} . \qquad (9)$$

It is a well known theorem that the loss-free, source-free magnetospheric diffusion of a power law spectrum of electrons, conserving μ and J and violating Φ, preserves the spectral index γ independent of r. Such an interpretation of Figure 8 is totally untenable. Also, as noted above, there is a virtually total absence of electrons between 0.040 and 0.56 MeV for $r < 5$. These facts suggest adopting a low energy cutoff E* in a power law spectrum such that the breaks in the curves at $r \sim 5$ occur at E* = 0.56 MeV, the energy threshold of B. The corresponding value of the first adiabatic invariant is called μ^*. Values of μ^* and γ, both assumed constant, are adopted as the parameters of an empirical fit to the observed data. The solid lines in Figure 8 show the calculated model fits with μ^* = 525 MeV/gauss and γ = 3.8 inbound and μ^* = 425 MeV/gauss and γ = 3.8 outbound. The fit was optimized over the radial ranges 2.3 - 7.8 inbound and 2.3 - 9 outbound. A change in μ^* by about 25 MeV/gauss or in γ by about 0.1 results in a perceptively poorer fit in both cases. It appears that significant absorption of low energy electrons (0.040 - 0.56 MeV)

occurs in the approximate radial range 8 - 12 (Figures 6 and 7). There is a corresponding change in the angular distribution of electrons $E_e > 0.040$ MeV (Panels 10 and 19 of Figure 6) (i.e., a relative depletion of particles at pitch angles $\alpha \sim 90°$). Electrons $E_e > 0.56$ MeV do not exhibit such changes (Figure 7). These effects are qualitatively consistent with the preferential depletion of low energy electrons (cf. a similar depletion in low energy protons (Figure 10 herein and Figure 2 of Paper I) by a low opacity ring of fine particulate material [Thomsen and Van Allen, 1979] or gas [Frank et al., 1980]. They are of the opposite nature to the effects of pitch angle scattering caused by interaction with whistler mode waves in a plasma [Sentman and Goertz, 1978].

The phase space density f of electrons as a function of r is shown in Figure 9. Here we have calculated, in the same approximate manner as for protons, the phase space density at $\mu = 525$ MeV/gauss (i.e., equal to the value of μ^* obtained by fitting the model spectrum to the inbound data of Figure 8) and with $\gamma = 3.8$. From the magnetopause (at $r \sim 17.3$) inward to $r \sim 10$, f is essentially constant but then declines by a factor of about 1000 to its value at $r \sim 5$. Sample values of E^* corresponding to $\mu^* = 525$ MeV/gauss are as follows:

(a) In the solar wind ($|B| \approx 0.3$ gamma), 0.0016 MeV;

(b) at r = 10, 0.099; (c) at r = 5, 0.56; and

(d) at r = 3, 1.59.

Our overall interpretation of Figure 9 is that the source of electrons $0.040 < E_e <$ (a few MeV) is external, presumably thermalized solar wind in the magnetosheath; that diffusion into $r \sim 10$ is relatively loss-free and source-free; and that at lesser radial distances there are very strong losses. We attribute the latter to an extended tenuous ring of particulate matter [Feibelman, 1967; Humes et al., 1980; IAUC No. 3476, 1980] and/or gas. General absorption of electrons by Mimas and by Rings G and F and the associated small satellites (except for absorption microsignatures of satellites [Paper I] [Thomsen et al., 1980]) is relatively slight. The inner boundary condition is complete absorption at the outer edge of Ring A [Paper I], though f has already reached a low value at $r \sim 5$.

Inner zone electrons from the decay of Crand neutrons (upper energy limit 0.78 MeV for a neutron at rest) are not perceptibly present.

SOURCES AND SINKS OF LOW ENERGY PROTONS ($E_p \sim 1$ MeV)

The radial dependence of the counting rate of detector G (protons $0.61 < E_p < 3.41$ MeV) is shown in Figure 3 and more fully in Figure 10, wherein the angular distributions are also shown. The unusually high abundance of interplanetary protons before and after the planetary encounter of Pioneer 11 is shown in Figure 11.

As shown in Figure 10, there is a mild decline of the counting rate of G inside of the magnetopause, then a strong increase beginning at $r \sim 15$. The maximum counting rate occurs at 7.5 and inward of this distance the counting rate goes to a very low value [cf. Figure 2 of Paper I]. Finally there is a narrow inner zone spike (both inbound and outbound) centered at 2.67, the position at which the intensity of protons $E_p > 80$ MeV has its maximum value. This inner zone spike is caused by the transverse penetration of the side-wall shielding and sensitive element of detector G by protons $E_p > 41$ MeV [Appendix B]. Elsewhere, detector G gives an unambiguous determination of the unidirectional intensity of protons in the energy range $0.61 < E_p < 3.41$ MeV, using the geometric factors of Table 2 to convert counting rate to absolute intensity.

On the basis of the radial dependence of the calculated phase space density of low energy protons (Figure 12), it is concluded that such protons have an external source and that the strong losses for $r < 10$ are attributable to absorption by Rhea, Dione, Tethys, and Enceladus and by a ring of fine particulate matter and/or gas.

Because of the fact that the magnetosphere of Saturn was immersed in an unusually high intensity of energetic solar protons during Pioneer 11's encounter period, the direct injection of such particles must be considered as a potential source, competitive with and perhaps more important than thermalized solar wind protons in the magnetosheath. The outbound intensity of low energy protons at $r \sim 7.5$ was about three times as great as the inbound intensity at the same radial distance and the angular distributions at these two points were qualitatively different (cf. panels 3 and 8 in the lower part of Figure 10). These facts suggest important temporal variations on a time scale of $\sim$ 10 hours. The extremely disturbed state of the solar wind at this time [Wolfe et al., 1980] gives further plausibility to this suggestion.

There is little doubt that protons of $E_p \sim 1$ MeV have an external source -- either the thermalized solar wind in the magnetosheath or solar energetic protons in the interplanetary medium or both -- with unknown relative importance. We have not yet been able to resolve this ambiguity.

SUMMARY

This paper reports the results of continuing analysis and interpretation of energetic particle observations obtained by the University of Iowa instrument on Pioneer 11 during traversal of Saturn's magnetosphere in August-September 1979. On the basis of the radial dependence of the phase space density of very energetic protons ($E_p > 80$ MeV) and estimates of the necessary source strength, it is reasonably certain that cosmic ray neutron albedo from the planet's atmosphere and Rings A and B is the source of such particles. At radial distance $r = 2.7\ R_s$ and for $E_p > 80$ MeV, the ratio of source strength β to radial diffusion coefficient D is $\sim 2 \times 10^{-24}\ cm^{-5}$. A reasonable pair of values is $\beta \sim 7 \times 10^{-15}\ cm^{-3}\ s^{-1}$ and $D \sim 1 \times 10^{-10}\ R_s^2\ s^{-1}$. The spectrum of electrons $0.040 < E_e <$ (a few MeV) and the radial dependence of the phase space density of such electrons are derived. The source of these electrons is at the magnetosheath. The source of protons $E_p \sim 1$ MeV is also at the magnetosheath and may be either thermalized solar wind or energetic interplanetary protons which were unusually abundant at the time of Pioneer 11's encounter. Low energy electrons and protons experience strong losses inward of $r \sim 10\ R_s$,

apparently attributable to the large inner satellites Rhea, Dione, Tethys, Enceladus, and Mimas and to a broad tenuous ring of particulate matter (Ring E) and/or gas. There were important temporal changes in the distributions of low energy electrons and protons within a period of ~ 10 hours between inbound and outbound passes, probably caused by unusually disturbed interplanetary conditions.

APPENDIX A

Description of University of Iowa Instrument and Other Observational Matters

Detectors: The system of detectors in our Pioneer 11 instrument is a modified and significantly improved version of that in our Pioneer 10 instrument. The characteristics and physical calibrations of the latter were described in detail in earlier papers [Baker, 1973; Van Allen et al., 1974; Baker and Van Allen, 1977]. For Pioneer 11, the changes in detectors were as follows:

(a) The shield in the collimator of detector A was removed so that only the thin mica window (1.2 mg/cm^2) of the Geiger-Mueller (GM) tube separated its sensitive volume from space. This change lowered its effective energy threshold to 0.040 MeV for electrons and 0.61 MeV for protons.

(b) Detector G (a GM tube in scatter geometry) in the Pioneer 10 instrument was replaced in its entirety by a thin, single element solid state detector with a physical collimator (also called G on Pioneer 11).

A cut-away view of an EON Corporation Type 6213 GM tube, used for detectors A, B, and C, is shown in Figure 13 and the physical arrangement of the three tubes is shown in Figure 14.

Individual counting rates of A, B, and C and multiple coincidence rates (1 μs resolving time) AB and ABC are transmitted. Note that the central tube C is shielded omnidirectionally, though not equally from all directions, whereas both A and B are shielded similarly from the side but are directional detectors, with the axes of their physical collimators (+X-axis) perpendicular to the rotational axis (+Z-axis) of the spacecraft. The differences in counting rates (A - C) and (B - C) are attributed to particles entering A and B, respectively, through their collimators. The fields of view shown in Figure 14 are nominal. The actual geometric factors of A, B, and C were determined experimentally as were their effective energy thresholds by the unit response method described previously [Van Allen et al., 1974].

The omnidirectionally shielded, triangular array of miniature GM tubes D, E, and F was the same on Pioneers 10 and 11. A cut-away view of an EON Corporation Type 5107 GM tube, as used for detectors D, E, and F, is shown in Figure 15 and the physical arrangement of the three identical tubes is shown in Figure 16. The individual counting rate of D and the triple coincidence rate (1 μs resolving time) DEF are transmitted.

The relationship between the apparent (i.e., observed) counting rate r and the rate R that would have been observed if the detector had zero dead-time was determined experimentally for each GM tube in the final flight configuation of the instrument

over the temperature range -30° to +35° C, a range considerably exceeding that experienced in flight. The temperature variation of the relationship was negligible. [Note, that in this section only the symbols r and R are used for counting rates; elsewhere in the paper r stands for radial distance.]

We had significant difficulty in making reliable dead-time corrections [Baker and Van Allen, 1977] to the GM tube data during the passages of Pioneers 10 and 11 through Jupiter's magnetosphere because of very high counting rates. However, the maximum apparent counting rates in Saturn's magnetosphere were very much less than those in Jupiter's magnetosphere and there were no significant problems with either dead-time or pulse pile-up effects.

Accurate and reliable dead-time corrections were made on each individual sample rate by using piecewise empirical fits to the laboratory r vs. R curves. The formulas that were used are given below. In each case an example is given for the greatest counting rate observed during the Saturn encounter.

Detector A

For $r < 1\,000$ c/s, $R = r$

$1\,000 < r < 2\,000$, $\ell n\, R = 1.104\, \ell n\, r - 0.718$;

$2\,000 < r < 3\,500$ $\ell n\, R = 6.718 + 4.774 \times 10^{-4}\, r$;

$3\,500 < r < 12\,000$ $\ell n\, R = 7.284 + 3.158 \times 10^{-4}\, r$.

Example: For $r = 7\,810$ c/s, $R = 17\,160$ c/s.

Detector B

For $r < 1\,000$ c/s, $R = r$;

$1\,000 < r < 1\,800$, $\ell n\, R = 1.092\, \ell n\, r - 0.635$;

$1\,800 < r < 2\,500$, $\ell n\, R = 6.480 + 5.942 \times 10^{-4}\, r$;

$2\,500 < r < 4{,}000$ $\ell n\, R = 6.933 + 4.129 \times 10^{-4}\, r$;

$4\,000 < r < 13\,900$ $\ell n\, R = 7.390 + 2.988 \times 10^{-4}\, r$.

Example: For $r = 7\,720$ c/s, $R = 16\,260$ c/s.

Detector C

For $r < 1\,000$ c/s, $R = r$;

$1\,000 < r < 1\,700$, $\ell n\, R = 1.210\, \ell n\, r - 1.451$;

$1\,700 < r < 3\,500$, $\ell n\, R = 6.674 + 5.149 \times 10^{-4}\, r$.

Example: For $r = 2\,990$ c/s, $R = 3\,690$ c/s.

Detectors D, E, and F

For $r < 1\,775$ c/s, $R = r$.

Example: For $r = 1\,140$ c/s, $R = 1\,140$ c/s. (Detector D)

All counting rate data in this paper are based on our Master Science File in which the counting rates are the fully corrected ones using the above formulae on each individual sample in the raw telemetry tape.

The sensitive element of detector G is a circular disc of totally depleted surface barrier silicon, $2.87\ (\pm 0.02) \times 10^{-3}$ cm in thickness and 0.122 ± 0.002 cm^2 in frontal area; both measurements were made experimentally. The mounting of the detector is shown in Figure 17. The axis of its physical collimator is also

the +X-axis, perpendicular to the rotational axis of the spacecraft and parallel to the axes of detectors A and B. An opaque double-layer nickel foil of total thickness 0.43 mg/cm^2 covers the outward face of the disc. Pulses from G are shaped to rectangular form by a delay line such that their time width is 0.18 μs, corresponding to a time resolution of 0.12 μs. There is a single electronic discrimination level at 0.53 MeV. This level was selected in the laboratory so that the lower energy threshold for protons (from a small Van de Graaff accelerator) was accurately matched to the proton threshold of detector A, namely 0.61 MeV. The upper energy cut-off was calculated from basic range-energy curves and the experimentally measured thickness of the disc. Thus, the energy window of this detector is $0.61 < E_p < 3.41$ MeV for protons and $0.88 < E_\alpha \leq 66$ MeV for alpha particles. For the electron intensities present in either Jupiter's or Saturn's magnetosphere, this detector is totally insensitive to electrons either singly or by pulse pile-up. Also R = r up to r = 10 000 c/s, a rate far above that observed in Saturn's magnetosphere. A weak Am^{241} alpha particle source (5.49 and 5.44 MeV) was provided for monitoring in-flight performance, giving a rate of 0.067 c/s. During quiet interplanetary conditions this "background" rate has been accurately constant for the nearly 6.5 years of flight enroute to Saturn. The only significant shortcoming of detector G is that it can be triggered by the transverse passage of high energy ($E_p > 41$ MeV) protons through

the side walls of its shield. An important consequence of this shortcoming is discussed in Appendix B (q.v.) in our interpretation of the narrow peaks in the counting rate of G inward of the orbit of Enceladus (Figures 3 and 10 herein and Figure 2 of Paper I). Elsewhere, the output of detector G is reliably attributable to protons $0.61 < E_p < 3.41$ MeV, entering the detector through its conical collimator. The nearly total absence of energetic ions having $Z \geq 2$ appears to be assured by multi-element solid-state telescope results from other Pioneer 11 instruments [Simpson et al., 1980; Trainor et al., 1980; McDonald, private communication, 1980].

An abridged summary of the characteristics of our several detectors is given in Table 2 of the text.

Telemetry and Sampling. During most of the Saturn encounter the spacecraft telemetry was operated in B/D format at a total bit rate of 512 b/s. (For several brief periods, a total bit rate of 1024 b/s was tried but the data quality was marginal.) The University of Iowa instrument uses 12 bits (4 words) in each 192-bit main science frame of the spacecraft's telemetry format (i.e., 6.25 percent of science telemetry). Quasi-logarithmic data compression is used to maintain one percent accuracy in all counting rates. All outputs are digital. A complete cycle of our data spans eleven main science frames as follows: sync word, G, A, B, G, AB, ABC, C, D, ABC, and DEF. The accumulation duty cycle is 9.1 percent for A, B, C, D, AB, and DEF and 18.2 percent for G and ABC. At a spacecraft bit rate of 512 b/s and format B/D, the accumulation

time for each of our samples is 0.75 s and the complete sampling cycle is completed in 8.25 s.

Angular Distributions. The +Z-axis of the rotating spacecraft is pointed continuously toward the earth to within 1°. During the Saturn encounter Pioneer 11's rotational period was 7.693 s. During each 0.75 s period, the axes of our detectors swept an angle of 35.1°; and in the interval 8.25 s between successive samples, 386.07°. Thus a complete angular distribution of nearly equally spaced samples over 360° of rotation was obtained each 14 cycles of data or 115.5 s. If one assumes mirror symmetry of particle intensity with respect to the plane normal to the local magnetic vector, seven cycles suffice.

In our basic reduction of angular distribution data, each data sample is labeled with the roll angle φ of the +X-axis of the spacecraft at the mid-time of accumulation of the sample. The roll angle φ is measured from the ascending node of the equator of the spacecraft on the ecliptic. The X-axis is parallel to the equatorial plane of the planet when $\varphi = 152°$ and 332° and parallel to the ecliptic plane when $\varphi = 0°$ and 180°. The mean pitch angle α of a given sample of data is derived from φ and the components of the local magnetic vector $\vec{B}$. The latter have been kindly supplied to us in convenient form by E. J. Smith et al., the HVM investigators.

APPENDIX B

Identification of Particle Species

The low energy proton threshold of G is accurately matched to that of the thin window Geiger-Mueller tube A. Also the angular responses of these two detectors are similar (Appendix A). Thus, because of the steeply falling proton energy spectrum for $E_p \sim 1$ MeV as measured during the Saturn encounter by other Pioneer 11 investigators, our counting rate quantity (A - C - kG) is reliably attributed solely to electrons of energy $E_e > 0.040$ MeV entering A through its physical collimator. The factor k (= 0.44) is the ratio of the unidirectional geometric factor of G to that of A (Table 2). Actually, the quantity kG/A is $\ll 1$ throughout the encounter and has been neglected.

Likewise for detector B, the counting rate difference (B - C) is reliably attributed solely to electrons of energy $E_e > 0.56$ MeV entering B through its physical collimator.

Identification of the radiation responsible for the counting rates of detectors C and D is a less straightforward process. The counting rates C and D and their ratio C/D are shown as a function of radial distance r inbound (Figure 18) and outbound

(Figure 19). The C/D vs r curves in both cases have a distinctive and revealing form. During periods of high C and D rates, C/D is essentially constant with a value of about 3.2. In the low counting rate (absorption) regions [Paper I] containing Ring F and satellites 1979 S5 and S6($2.34 < r < 2.37$); Ring G and satellites 1979 S2 and S4 ($2.49 < r < 2.55$); and Mimas' orbit ($3.03 < r < 3.16$); and for $r > 3.6$, C/D rises to a distinctly greater value, about 4.5 to 5.0. The interplanetary value of C/D for the very penetrating cosmic radiation is 3.75. This value is taken to be the true ratio of the omnidirectional geometric factors of the two detectors. For penetrating but less energetic protons, the energy thresholds of detectors C and D are about the same (E_p = 80 MeV) and a similar ratio may be expected, though the complex nature of the shielding makes the calculation of this ratio somewhat uncertain and in mild disagreement with either 3.2 or 3.75 (cf. Table 2). The DEF/D ratio provides an additional diagnostic. At $r \sim 2.66$, the observed value of this ratio is 6×10^{-4}, a value too low by about a factor of 20 for penetrating electrons but reasonable for penetrating protons of ~ 100 MeV energy [Baker, 1973]. Also the radial width of the wings of Mimas' absorption macrosignature, as well as those of the absorption signatures of Rings G and F (Figures 18 and 19) are about twice the gyroradius of protons $E_p \sim 100$ MeV, a necessary but not sufficient condition for attributing the responses of C and D dominantly to penetrating protons. On the basis of these various considerations we consider it reasonably certain that

the high counting rates of C and D in the regions corresponding to the "base" ratio C/D ~ 3.2 in Figures 18 and 19 are caused by penetrating protons $E_p > 80$ MeV.

In the absorption regions, in which the C/D ratio has its higher value, the causative radiation can not be penetrating protons. The most conclusive evidence to this effect is that the radial widths of the absorption microsignature of Mimas [Thomsen et al., 1980] at r = 3.065 and the absorption signatures of satellites 1979 S2, S4, S5, and S6 (Paper I) are less than four gyroradii for protons $E_p \sim 100$ MeV by a factor of 10 to 100. We conclude that there are essentially no penetrating protons in these regions, a result consistent with Figure 5 of Fillius et al. [1980]. The residual counting rates of C and D in these absorption regions may be caused by either penetrating electrons ($E_e > 21$ MeV for C and $E_e > 31$ MeV for D) (Table 2) or by the bremsstrahlung from non-penetrating electrons. The gyroradii of penetrating electrons are moderately, but not conclusively, incompatible with the radial widths of the observed satellite signatures cited above. However, our interpretation of Mimas' absorption microsignature [Thomsen et al., 1980] is totally incompatible with electrons of energies of 20-30 MeV. Also electrons of the necessary energy to penetrate the shields of detectors C and D are theoretically unlikely (see Sources and Sinks of Electrons); and on an empirical basis, the necessary intensities

of penetrating electrons are about an order of magnitude greater than would be expected from the spectral form inferred from the (A - C)/(B - C) and (B - C)/C ratios.

All of the foregoing considerations favor the interpretation that the responses of C and D in the absorption regions are caused primarily by bremsstrahlung resulting from the bombardment of the instrument by non-penetrating electrons. The absolute γ-ray efficiencies of C and D in the final flight configuration were measured in pre-flight tests with a 5,000 curie Co^{60} source (E_γ = 1.173 and 1.332 MeV). The remaining quantitative link in this interpretative chain is the computation of the absolute thick-target bremsstrahlung spectrum [Evans, 1955] resulting from the electron spectrum inferred from the (A - C)/(B - C) ratios. In full practical detail, this calculation is quite complex but rough estimates support the bremsstrahlung interpretation to within a factor of two.

For radial distances $r \geq 4$ the response of our solid state detector G is attributable solely to protons $0.61 < E_p < 3.41$ MeV, entering the detector through its conical collimator (Appendix A).

However, in the inner radiation zone ($r \leq 4$), its response is largely or wholly attributable to the transverse penetration of the side-wall shield and the sensitive element of the detector by protons $E_p > 41$ MeV. Thus, the three inner zone peaks in the curve of G's counting rate vs r [Figure 2 of Paper I]

are "spurious" in the sense that they do not correspond to the nominal characteristics of G as given in Table 2, even though the detector is operating reliably. The following evidence for this conclusion refers principally to the major inner zone peak centered at $r \sim 2.67$ (both inbound and outbound) because the counting rate statistics in this peak are superior to those in the smaller peaks on either side. However, the conclusion appears to be applicable to all three peaks.

(a) Through the major peak ($2.95 > r > 2.57$) the spin-averaged counting rates of both C and G vary by a factor of about ten but the C/G ratio is accurately constant at a mean value of 240, suggesting that the two quite disparate detectors are sampling the same population of protons.

(b) Despite the fact that detectors C and D are omnidirectional in nature, there is a significant roll angle modulation in their counting rates [Figure 4 of Paper I] because of lack of spherical symmetry of the detectors themselves and of their shields. A detailed study of the roll phase of this modulation shows that the angular distribution of protons $E_p > 80$ MeV is of pancake form having maximum intensity at pitch angle $\alpha = 90°$ and with $j \propto \sin^4 \alpha$.

(c) On the other hand, the apparent angular distribution of the particles causing G's response is of dumbbell form having a maximum when the axis of G is parallel to the local magnetic

vector, in contrast to the situation in the outer radiation zone. The apparent angular distributions for G are shown in Figure 10; index numbers 5 and 6 mark the major inner zone maximum.

(d) Combining our detector C and detector D data on protons $E_p > 80$ MeV with the University of California, San Diego data [Fillius et al., 1980] for the same energy threshold and with the University of Chicago data [Simpson et al., 1980] for $E_p > 35$ MeV we find a crude differential energy spectrum of the form $j \propto E^{-1.5}$ in this spectral region.

(e) Then, using the detailed geometric and physical properties of our detector G, we calculate the expected counting rate of G due to "cross-fire" of penetrating protons through its shield and sensitive element [cf. Krimigis and Van Allen, 1967]. The expected absolute counting rates due to cross-fire are found to agree with those observed to within about 20 percent and the apparent dumbbell angular distribution is accurately reproduced.

ACKNOWLEDGEMENTS

This work was supported in part by Ames Research Center/ National Aeronautics and Space Administration contract NAS2-6553 and by the U. S. Office of Naval Research. The authors are indebted to C. F. Hall, J. H. Wolfe, J. W. Dyer, R. O. Fimmel, and many others of the ARC for making this work possible; to R. L. Rairden and C. L. Grosskreutz of the University of Iowa for assistance in analysis; to R. F. Randall, H. D. Owens, and D. E. Cramer of the University of Iowa for engineering such a durable and reliable instrument (1968-1973); and to E. J. Smith of the Jet Propulsion Laboratory for the detailed magnetic field data used in our work.

REFERENCES

Acuna, M. H., and N. F. Ness, The magnetic field of Saturn: Pioneer 11 observations, Science, 207, 444, 1980.

Baker, D. N., University of Iowa Pioneer 10 and 11 instrument calibration, University of Iowa Research Report 73-26, 1973.

Baker, D. N., and J. A. Van Allen, Revised Pioneer 10 absolute electron intensities in the inner Jovian magnetosphere, J. Geophys. Res., 82, 681, 1977.

Evans, R. D., The Atomic Nucleus, McGraw-Hill, New York, 1955.

Feibelman, W. A., Concerning the D′ [E] ring of Saturn, Nature, 214, 793, 1967.

Fillius, W., W. H. Ip, and C. E. McIlwain, Trapped radiation belts of Saturn: First look, Science, 207, 425, 1980.

Frank, L. A., B. G. Burek, K. L. Ackerson, J. H. Wolfe, and J. D. Mihalov, Plasmas in Saturn's magnetosphere, J. Geophys. Res., 85, this issue, 1980.

Hess, W. N., The Radiation Belt and Magnetosphere, Blaisdell Pub. Co., Waltham, MA, 1968.

Humes, D. H., R. L. O'Neal, W. H. Kinard, and J. M. Alvarez, Impact of Saturn ring particles on Pioneer 11, Science, 207, 443, 1980.

International Astronomical Union Circular No. 3476 of 12 May 1980.

Krimigis, S. M., and J. A. Van Allen, Geomagnetically trapped alpha particles, J. Geophys. Res., 72, 5779, 1967.

Orton, G. S., and A. P. Ingersoll, Saturn atmospheric temperature structure and heat budget, J. Geophys. Res., 85, this issue, 1980.

Roederer, J. G., Dynamics of Geomagnetically Trapped Radiation, Springer-Verlag, Heidelberg-New York, 1970.

Sauer, H. H., On Saturnian cosmic ray cutoff rigidities, Geophys. Res. Lett., 7, 215, 1980.

Schulz, M., and L. J. Lanzerotti, Particle Diffusion in the Radiation Belts, Springer-Verlag, Berlin, 1974.

Sentman, D. D., and C. K. Goertz, Whistler mode noise in Jupiter's inner magnetosphere, J. Geophys. Res., 83, 3151, 1978.

Simpson, J. A., T. S. Bastian, D. L. Chenette, G. A. Lentz, R. B. McKibben, K. R. Pyle, and A. J. Tuzzolino, Saturnian trapped radiation and its absorption by satellites and rings: The first results from Pioneer 11, Science, 207, 411, 1980.

Smith, E. J., L. Davis, Jr., D. E. Jones, P. J. Coleman, Jr., D. S. Colburn, P. Dyal, and C. P. Sonett, Saturn's magnetic field and magnetosphere, Science, 207, 407, 1980.

Thomsen, M. F., and J. A. Van Allen, On the inference of properties of Saturn's Ring E from energetic charged particle observations, Geophys. Res. Lett., 6, 893, 1979.

Thomsen, M. F., J. A. Van Allen, and B. A. Randall, The energetic charged particle absorption signature of Mimas, J. Geophys. Res., 85, this issue, 1980.

Trainor, J. H., F. B. McDonald, and A. W. Schardt, Observations of energetic ions and electrons in Saturn's magnetosphere, Science, 207, 421, 1980.

Van Allen, J. A., D. N. Baker, B. A. Randall, and D. D. Sentman, The magnetosphere of Jupiter as observed with Pioneer 10. 1. Instrument and principal findings, J. Geophys. Res., 79, 3559, 1974.

Van Allen, J. A., M. F. Thomsen, B. A. Randall, R. L. Rairden, and C. L. Grosskreutz, Saturn's magnetosphere, rings, and inner satellites, Science, 207, 415, 1980. [Paper I]

White, R. S., High-energy proton radiation belt, Rev. Geophys. Space Phys., 11, 595, 1973.

Wolfe, J. H., J. D. Mihalov, H. R. Collard, D. D. McKibbin, L. A. Frank, and D. S. Intriligator, Preliminary results on the plasma environment of Saturn from the Pioneer 11 plasma analyzer experiment, Science, 207, 403, 1980.

Table 1

Summary of Events During
Pioneer 11's Encounter with Saturn

Event	ERT/DOY (Note 1)	r (Note 2)
Bow Shock (Note 3)	1207-1816/243	24.1 - 20.0
Magnetopause (Note 3)	2209/243	17.3
Ring Plane Crossing	1555/244	2.928
Outer Edge of Ring A	1632/244	2.292
Periapsis	1757/244	1.349
Occultation by Planet (Note 4)		
Ingress	1758/244	1.350
Egress	1916/244	2.210
Outer Edge of Ring A	1921/244	2.292
Ring Plane Crossing	1950/244	2.774
Magnetopause (Note 3)	0917/246 - 0104/247	30.3 - 39.8
Bow Shock (Note 3)	1653/247 - 1530/251	49.3 - 102.1

Notes:

1. ERT is the universal time (UT) of reception of the telemetry signal at the earth. The relationship between ERT and ephemeris time at the spacecraft ET (S/C) varies by a few seconds during the encounter. At periapsis the relationship is:
   ERT = ET (S/C) - $50^{s}.2$ + 86^{m} $20^{s}.7$.
   DOY is the day of year 1979 (e.g., DOY 244 = 1 September).

Notes (continued)

2. Radial distances of the spacecraft from the center of Saturn are given in units of the adopted equatorial radius of the planet, 1 R_S = 60,000 km.

3. Wolfe et al. [1980].

4. Calculated from the spacecraft ephemeris assuming that the planet is spherical with radius 60,000 km.

5. No occultation by the rings occurred.

6. The plane of the hyperbolic encounter trajectory was inclined 6°.6 to the equatorial plane (ring plane) of the planet.

7. The adopted polar axis of the planet has longitude λ = 78°.8142 and latitude β = 61°.9324 in mean ecliptic-equinox coordinates of 1950.0.

Table 2

University of Iowa/Geiger Tube Telescope
Energy Ranges and Geometric Factors of Pioneer 11 Detectors

Detector	Effective Energy Range, MeV	Effective Inverse Omnidirectional Geometric Factor (1/Q), cm^{-2}	Type	$\frac{1}{4\pi Q}$ $(cm^2\ sr)^{-1}$
		Electrons		
A - C	$0.040 < E_e < 21$	730	Directional	58.1
B - C	$0.56 < E_e < 21$	785	Directional	62.5
G	Insensitive to electrons of any energy	-	-	-
C	$E_e > 21$	23	Omnidirectional	-
D	$E_e > 31$	63	Omnidirectional	-
		Protons		
A - C	$0.61 < E_p < 80$	650	Directional	51.7
B - C	$9 < E_p < 80$	650	Directional	51.7
G	$0.61 < E_p < 3.41$	285	Directional	22.7
C	$E_p > 80$	8.2	Omnidirectional	-
D	$E_p > 80$	23	Omnidirectional	-

Note 1. The absolute omnidirectional intensity J in $(cm^2\ sec)^{-1}$ is approximated by the product of the spin-averaged counting rate by (1/Q). The absolute unidirectional intensity j in $(cm^2\ sec\ sr)^{-1}$ is the product of the counting rate by $(1/4\pi Q)$.

Note 2. The quoted geometric factors include the intrinsic efficiency of detection by the sensitive element of each detector.

FIGURE CAPTIONS

Figure 1. Planet-centered equatorial plane projection of the trajectory of Pioneer 11 during its encounter with Saturn. The spacecraft entered the magnetosphere near local noon and exited near dawn. It was north of the equatorial plane along the solid line and south, along the dashed line. The positions of seven major satellites during the encounter are shown by curved arrows; the tail of each arrow is the position of the satellite at the time Pioneer crossed its orbit inbound, and the head of the arrow is its position at the time Pioneer crossed its orbit outbound [Van Allen et al., 1980].

Figure 2. Meridian plane projection of Pioneer 11's trajectory during its encounter with Saturn. The cross hatching shows the time period during which the spacecraft was occulted by the planet.

Figure 3. Overview of University of Iowa observations during the traversal of Saturn's magnetosphere. Displayed are 15-minute averages of the fully corrected counting rates of detectors A, B, C, D, and G. Thick vertical bars indicate encounters with the bow shock (BS) and magnetopause (MP).

Thinner vertical bars indicate the times at which the orbits of previously known satellites were crossed. The scale of radial distance is at the top of the diagram [Van Allen et al., 1980].

Figure 4. Radial dependence of the phase space density f (in arbitrary units) of high energy protons as derived from the observed counting rate of detector C. A differential spectral index $\gamma = 1.3$ was assumed and f was calculated for a constant value of the first adiabatic invariant $\mu = 8.137 \times 10^3$ MeV/gauss and a zero value of the second adiabatic invariant J.

Figure 5. A diagram to illustrate the geometric basis for calculating the source strength of cosmic ray neutron albedo decay (Crand) at an external point P. $I(\theta,\zeta,\psi)$ represents the directional intensity of albedo neutrons emitted upward per unit solid angle per unit area per unit time at colatitude θ, zenith angle ζ and azimuth ψ from the upper atmosphere of a planet of radius a.

Figure 6. (Top Panel) Fourteen sample (115.5 seconds) average counting rates of detector A during Saturn encounter. The inbound crossing and first outbound crossing of the magnetopause (MP) are indicated by heavy vertical bars. Lighter vertical bars are numbered to correspond to individual pitch angle distributions shown in the bottom panel. Absolute

intensities can be derived from the counting rates by Table 2 and Appendix A. The scale of radial distance is at the top of the diagram. (Center Panel) Amplitude of the second order Fourier component of the roll angle distribution determined from fits to 15 minute blocks of data. (Bottom Panel) Sample pitch angle distributions observed by detector A. Each represents 131 seconds of data. The radial distance at which each distribution was observed is shown in the upper left-hand corner, and the center time of the interval is shown in the upper right. The distributions have been normalized to a running average of the counting rate to eliminate the effects of temporal trends in the overall intensity.

Figure 7. Same as Figure 6 but for detector B.

Figure 8. The ratio of the counting rates of detectors A and B (each minus the rate of detector C) as a function of radial distance for the inbound and outbound portions of the Saturn encounter. The dots are the observed values, and the solid curves are derived from a model as described in the text.

Figure 9. Radial dependence of the phase space density (in arbitrary units) of electrons at constant first adiabatic invariant derived from the inbound counting rates of detectors A and B (each minus the rate of detector C) assuming a power law spectrum with a cutoff at a value of $\mu^* = 525$ MeV/gauss.

Figure 10. Same as Figure 6 but for detector G.

Figure 11. Counting rates of detectors A, B, and G just before and just after the encounter with Saturn. The quiet interplanetary counting rates of these detectors are about 1.0, 1.0, and 0.067 s^{-1}, respectively. The large enhancements in the counting rates of A and G are attributed to a solar energetic particle event which was in progress during the encounter.

Figure 12. Radial dependence of phase space density (in arbitrary units) of protons at constant first adiabatic invariant derived from the inbound counting rate of our detector G assuming a power law spectrum with values of the differential spectral index γ from the work of Trainer et al. [1980].

Figure 13. Cut-away view of an EON Corporation Type 6213 Geiger-Mueller tube identical to those used for detectors, A, B, and C.

Figure 14. Physical arrangement of detectors A, B, and C. The rotational axis of the spacecraft is the +Z axis.

Figure 15. Cut-away view of an EON Corporation Type 5107 Geiger-Mueller tube identical to those used for detectors D, E, and F.

Figure 16. Physical arrangement of the omnidirectionally shielded array of detectors D, E, and F.

Figure 17. Cut-away view of the mounting of detector G.

Figure 18. Counting rates of detectors C and D and the ratio C/D as a function of radial distance for the inbound portion of the encounter. The range of radial distance covered by Mimas in its slightly eccentric orbit is shown as a horizontal bar.

Figure 19. Same as Figure 18, but for the outbound portion of the encounter.

C-G79-351

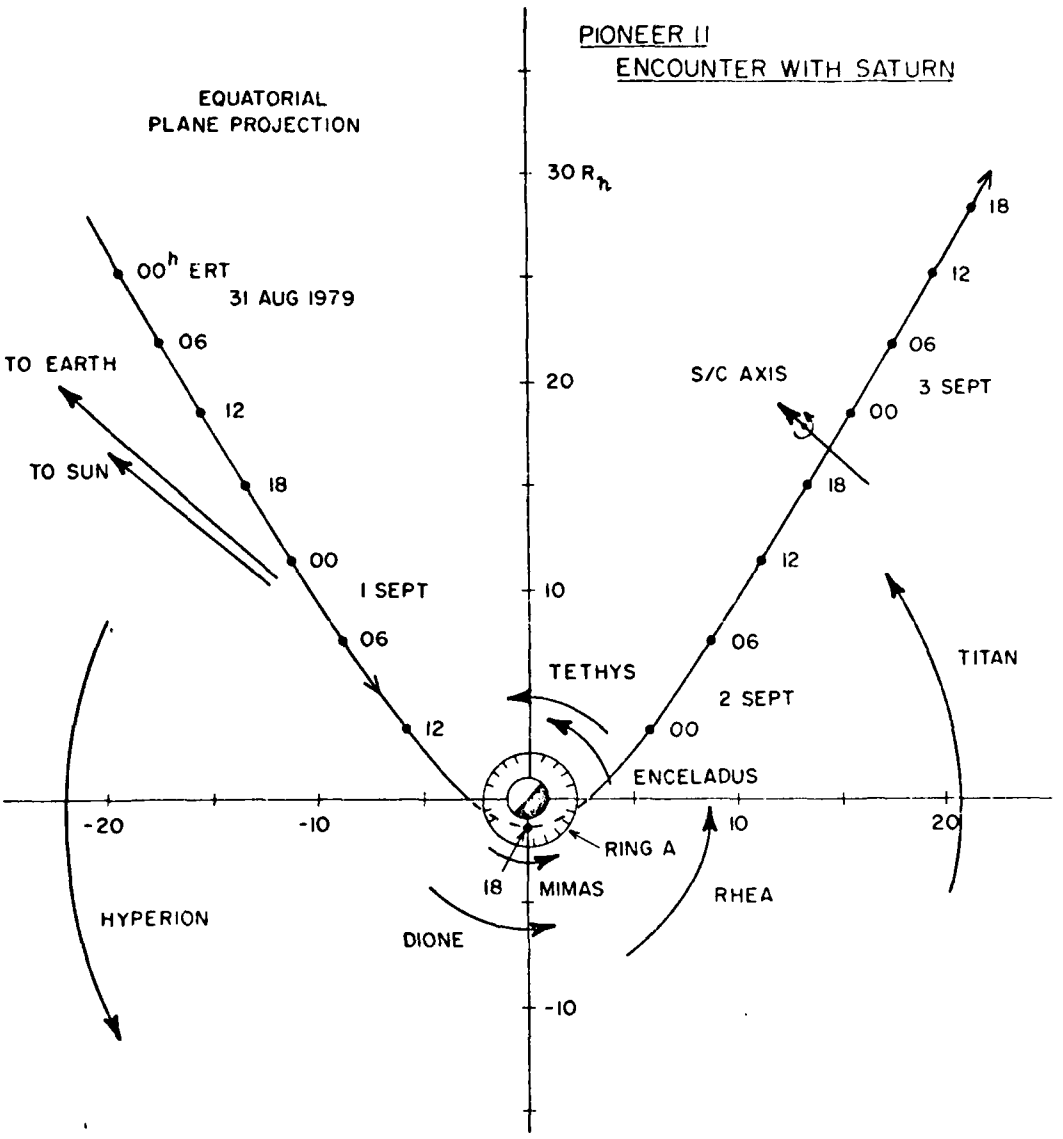

Figure 1

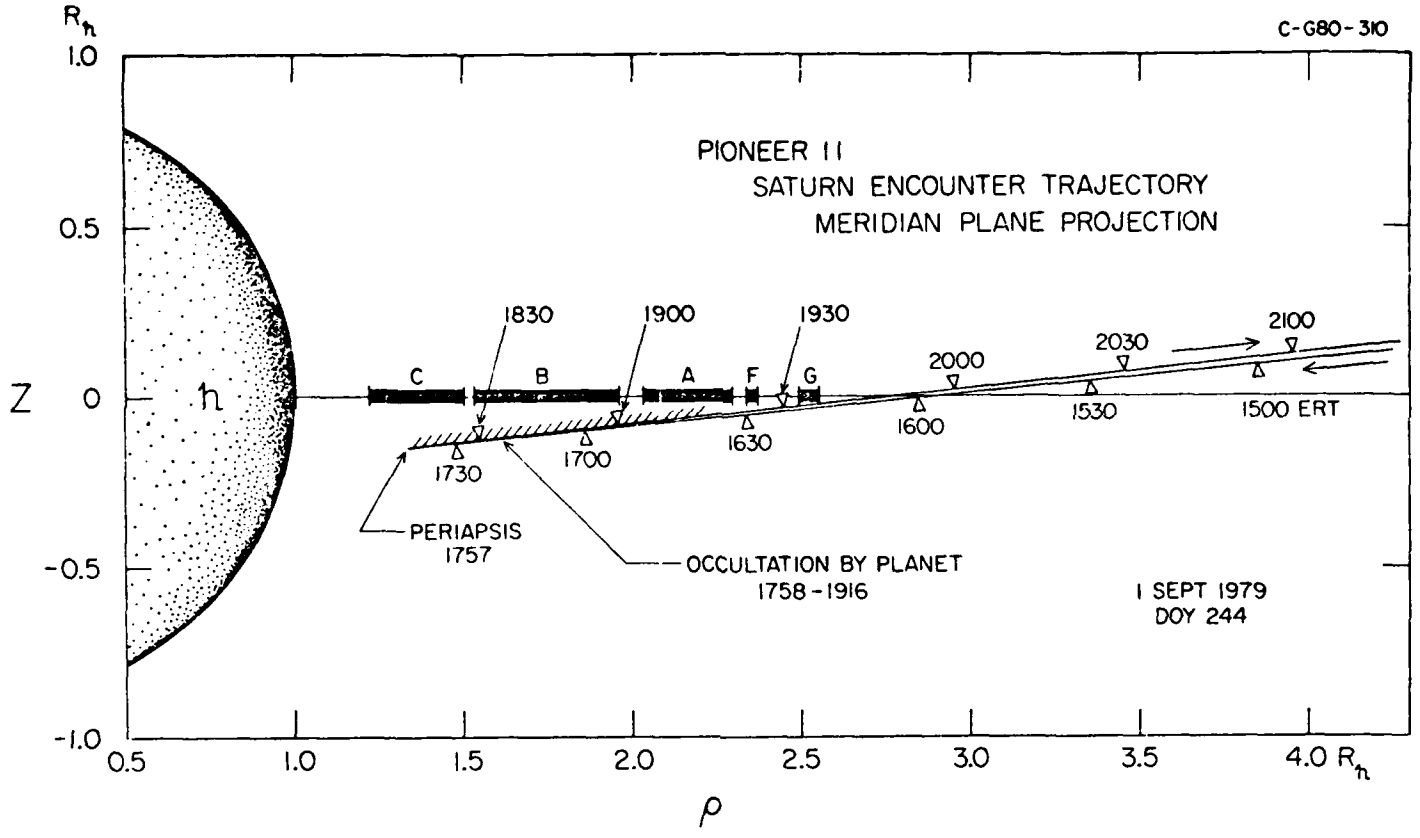
C-G80-310
PIONEER 11
SATURN ENCOUNTER TRAJECTORY
MERIDIAN PLANE PROJECTION
R_h
1.0
0.5
Z 0
h
-0.5
-1.0
0.5
1.0
1.5
2.0
2.5
3.0
3.5
4.0 R_h
ρ
C
B
A
F
G
1830
1900
1930
2000
2030
2100
1730
1700
1630
1600
1530
1500 ERT
PERIAPSIS
1757
OCCULTATION BY PLANET
1758 - 1916
1 SEPT 1979
DOY 244

Figure 2

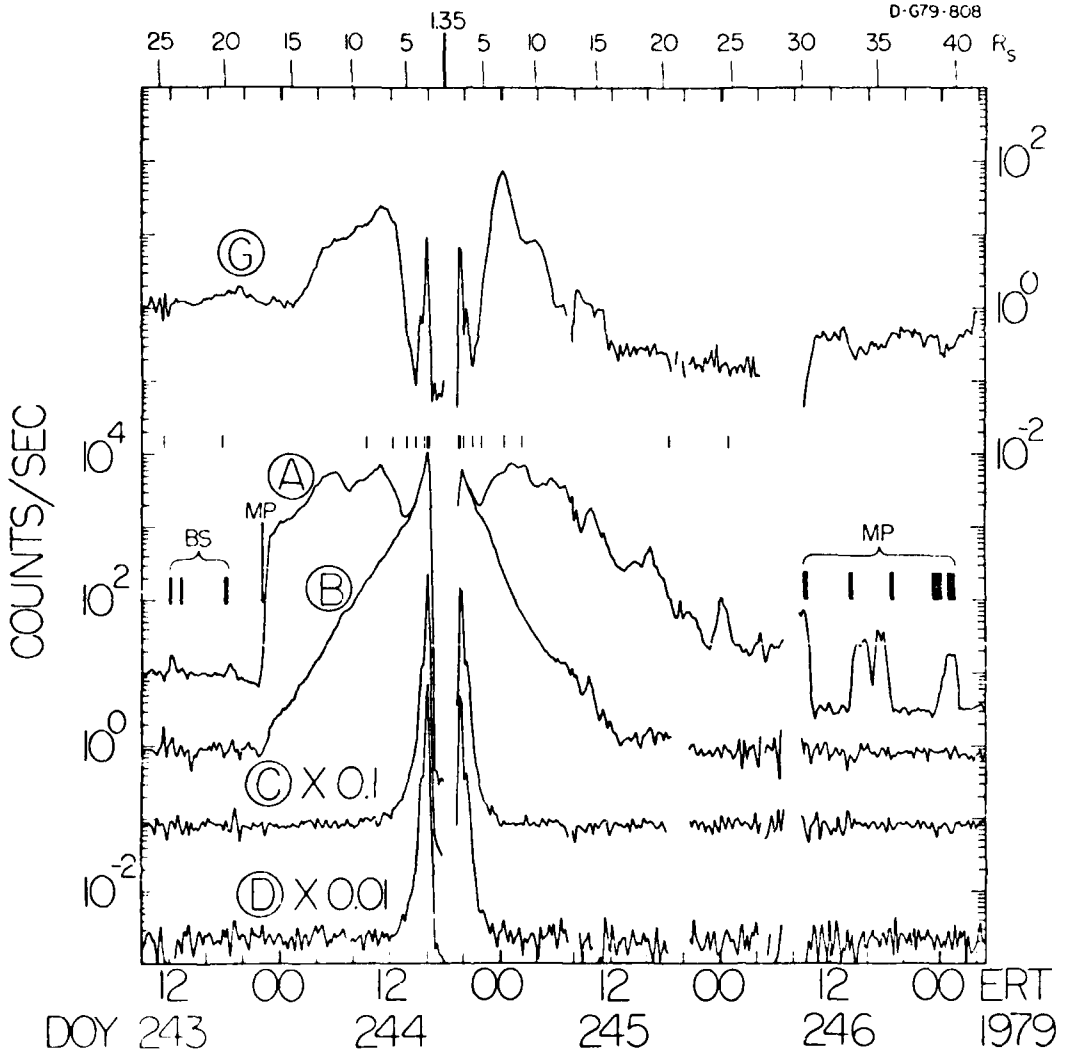
D-G79-808
1.35
25 20 15 10 5 5 10 15 20 25 30 35 40 R_S
G
A
B
C X 0.1
D X 0.01
MP
BS
MP
COUNTS/SEC
10^4
10^2
10^0
10^{-2}
10^2
10^0
10^{-2}
12 00 12 00 12 00 12 00 ERT
DOY 243 244 245 246 1979

Figure 3

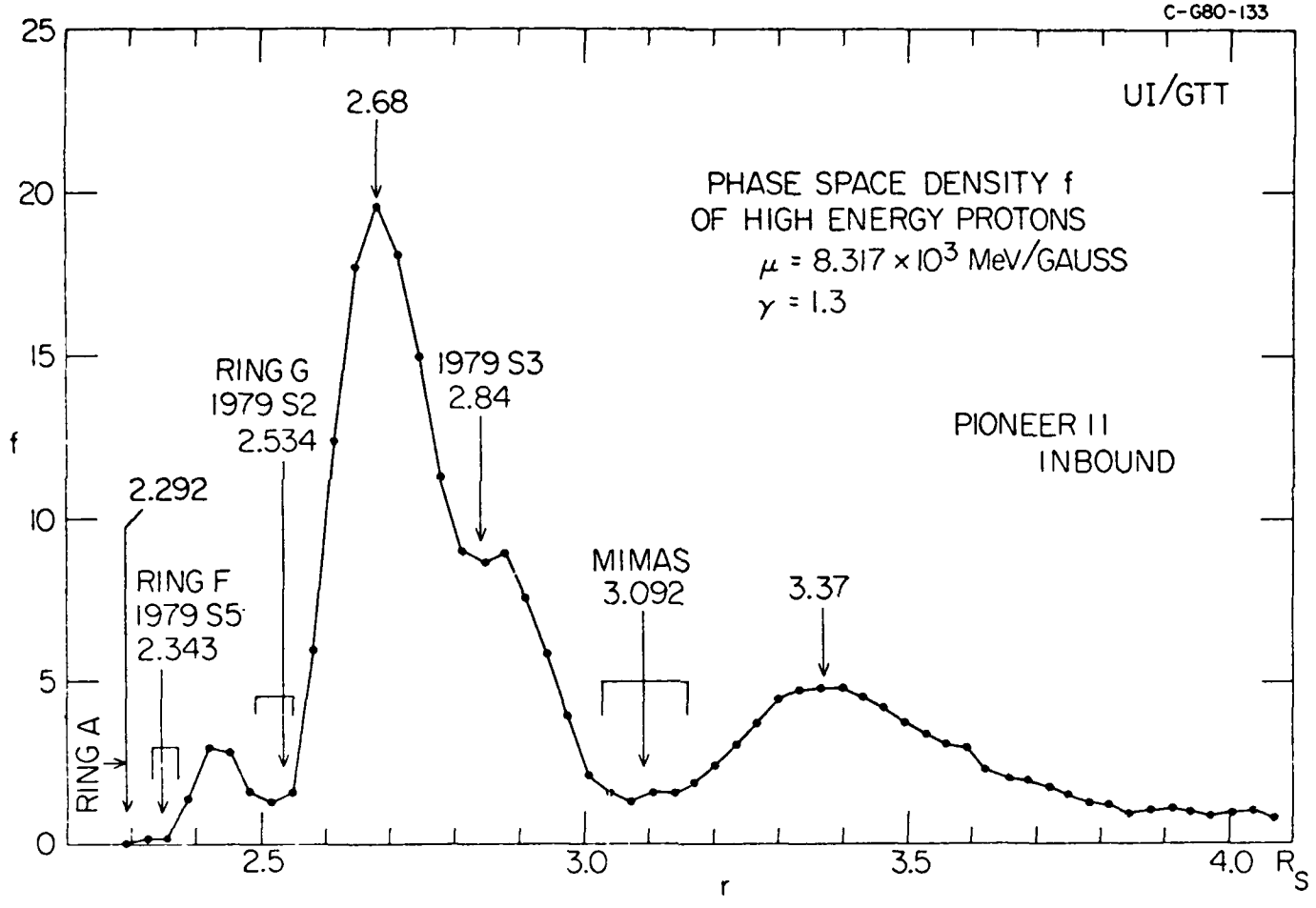
C-G80-133
UI/GTT
PHASE SPACE DENSITY f
OF HIGH ENERGY PROTONS
$\mu = 8.317 \times 10^3$ MeV/GAUSS
$\gamma = 1.3$
PIONEER 11
INBOUND
2.68
RING G
1979 S2
2.534
1979 S3
2.84
2.292
RING F
1979 S5
2.343
RING A
MIMAS
3.092
3.37
f
r
R_S
0
5
10
15
20
25
2.5
3.0
3.5
4.0

Figure 4

A-G80-402

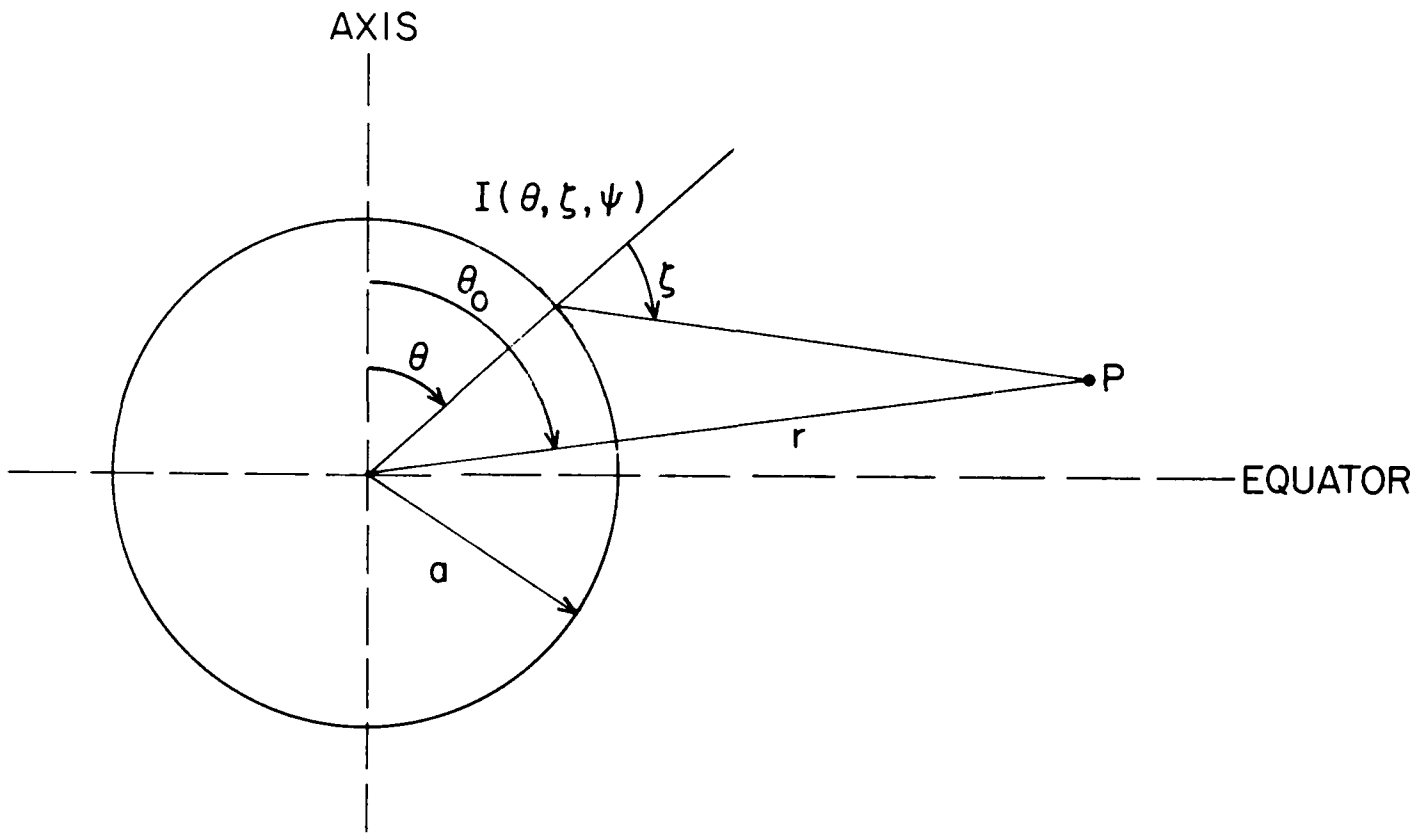

Figure 5

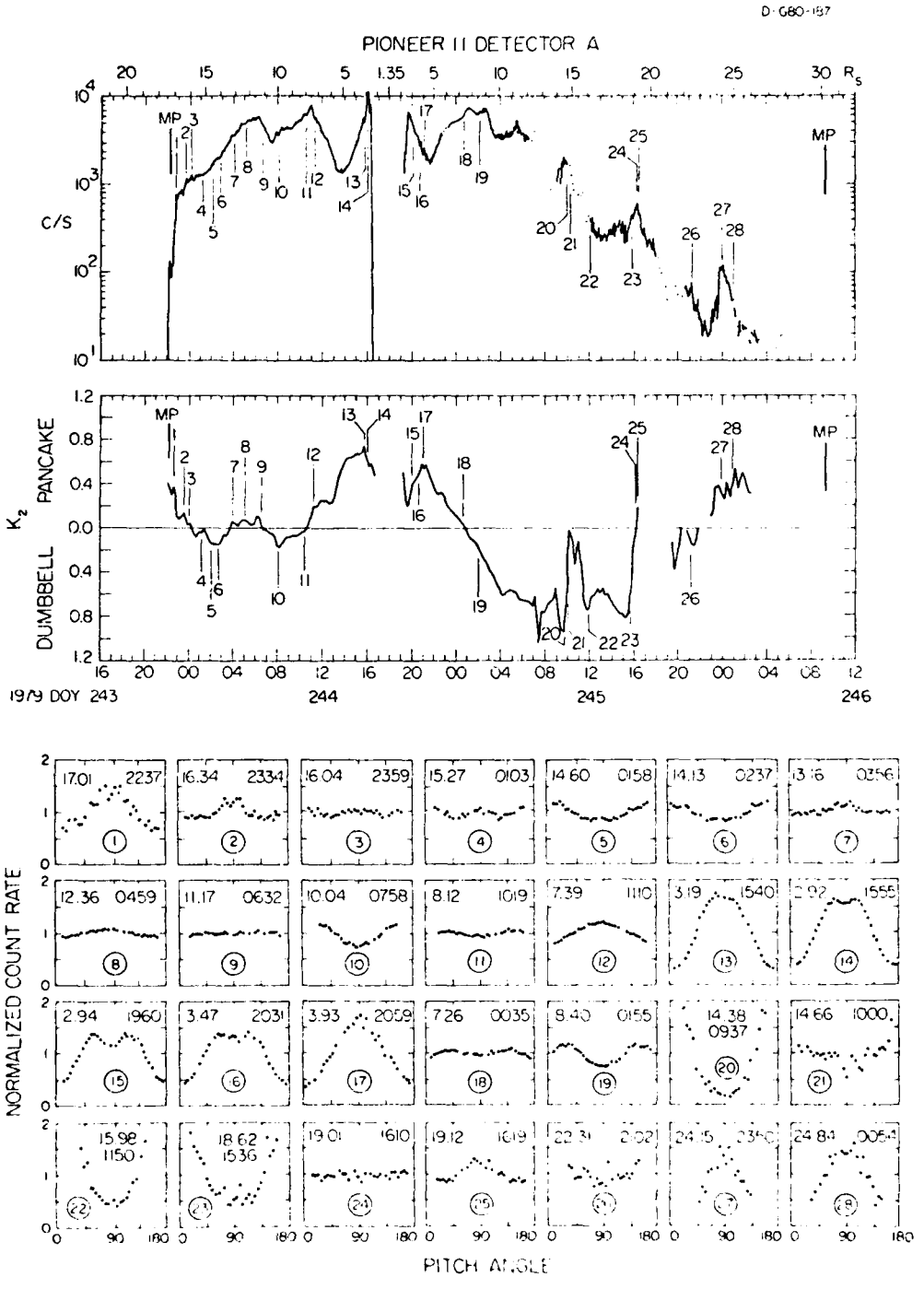
D-680-187
PIONEER 11 DETECTOR A
C/S
K_2
PANCAKE
DUMBBELL
1979 DOY 243
244
245
246
NORMALIZED COUNT RATE
PITCH ANGLE

Figure 6

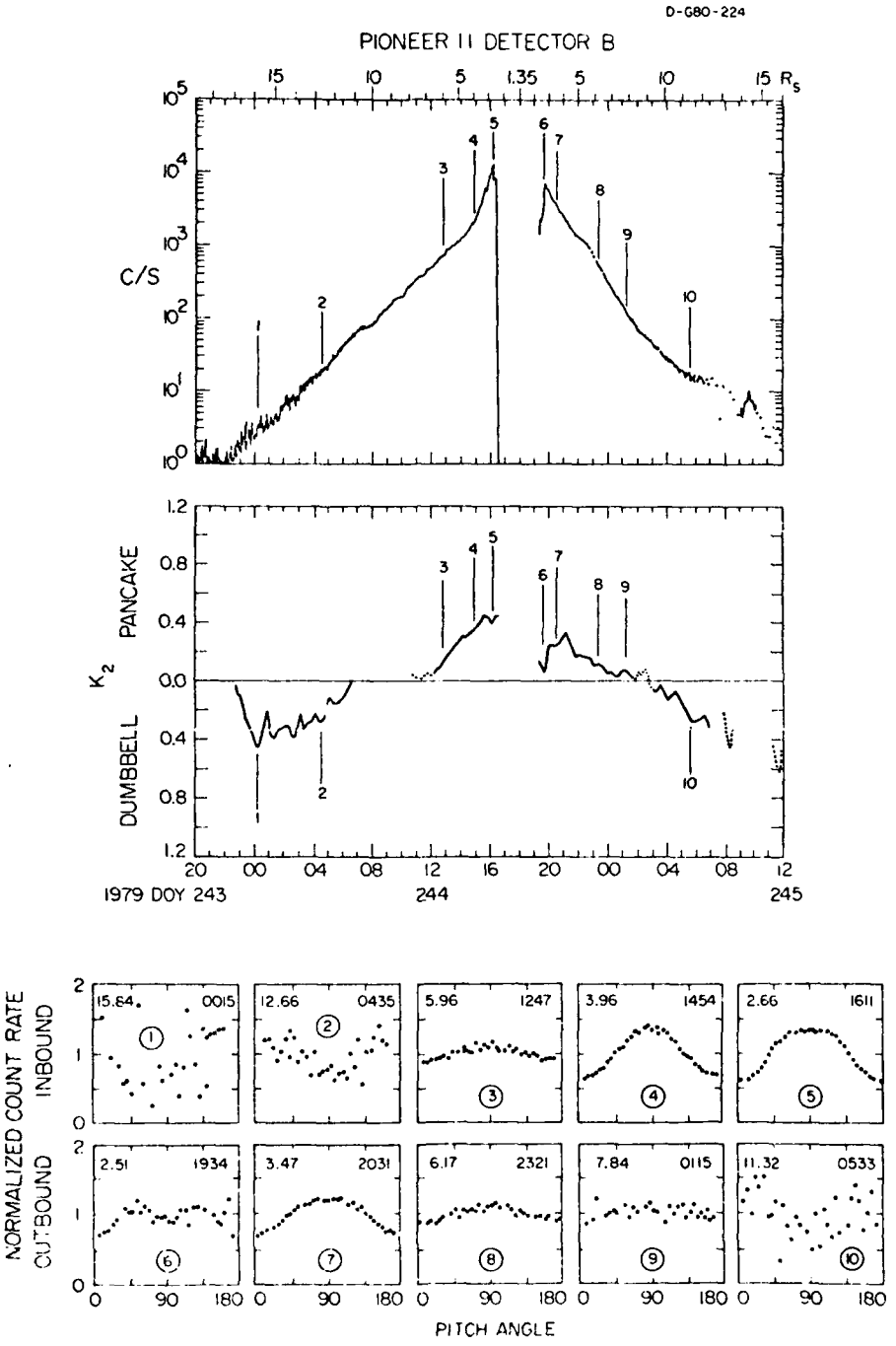
D-G80-224
PIONEER 11 DETECTOR B
15 10 5 1.35 5 10 15 R_S
C/S
10^5
10^4
10^3
10^2
10^1
10^0
1 2 3 4 5 6 7 8 9 10
K_2
PANCAKE
DUMBBELL
1.2 0.8 0.4 0.0 0.4 0.8 1.2
20 00 04 08 12 16 20 00 04 08 12
1979 DOY 243
244
245
NORMALIZED COUNT RATE
INBOUND
OUTBOUND
2
1
0
15.64 0015 ①
12.66 0435 ②
5.96 1247 ③
3.96 1454 ④
2.66 1611 ⑤
2.51 1934 ⑥
3.47 2031 ⑦
6.17 2321 ⑧
7.84 0115 ⑨
11.32 0533 ⑩
0 90 180
PITCH ANGLE

Figure 7

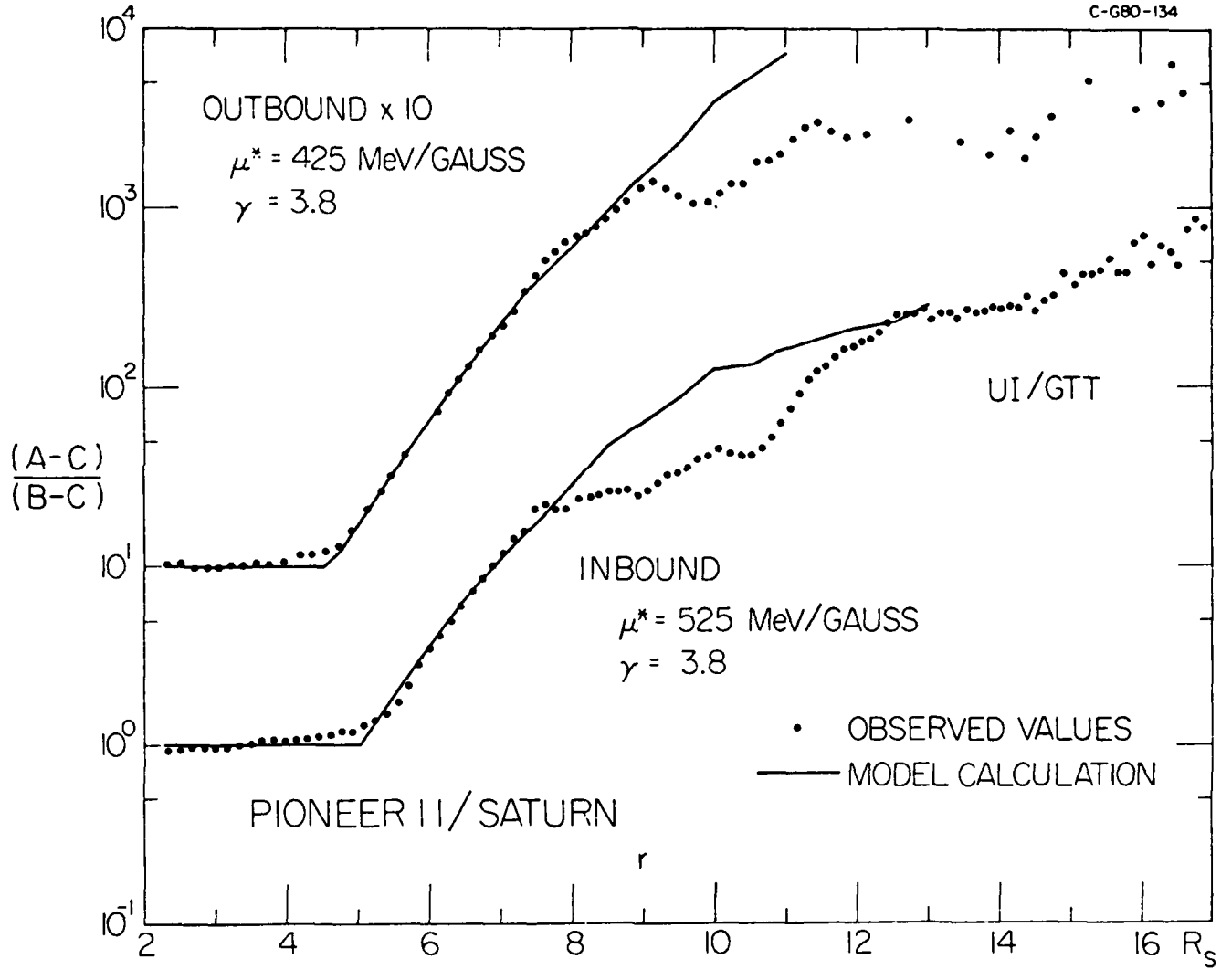
C-G80-134
OUTBOUND x 10
μ^* = 425 MeV/GAUSS
γ = 3.8
UI/GTT
INBOUND
μ^* = 525 MeV/GAUSS
γ = 3.8
• OBSERVED VALUES
—— MODEL CALCULATION
PIONEER 11/SATURN
r
$\frac{(A-C)}{(B-C)}$
10^4
10^3
10^2
10^1
10^0
10^{-1}
2
4
6
8
10
12
14
16 R_S

Figure 8

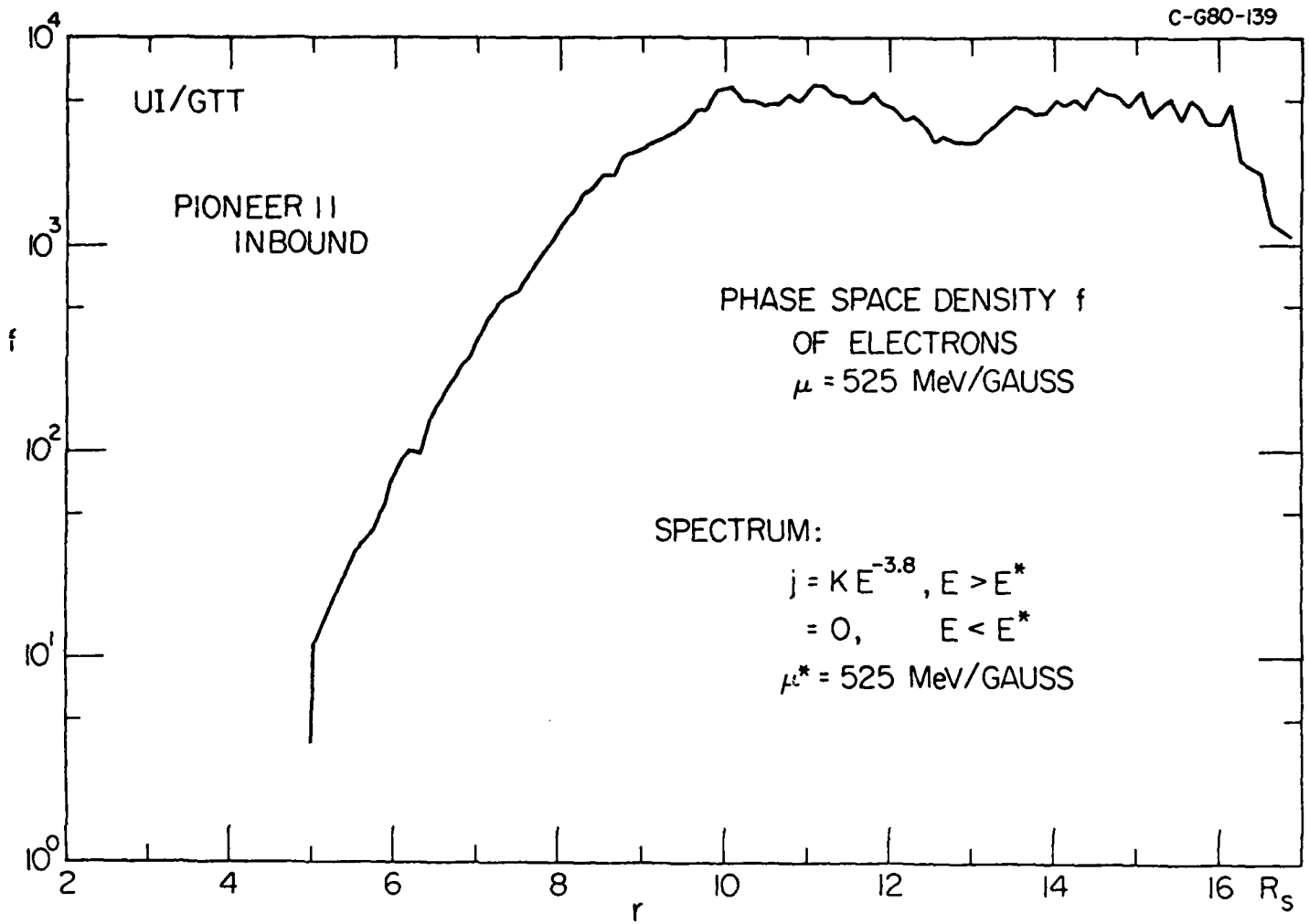
C-G80-139
UI/GTT
PIONEER 11
INBOUND
PHASE SPACE DENSITY f
OF ELECTRONS
μ = 525 MeV/GAUSS
SPECTRUM:
j = K E^-3.8 , E > E*
= 0, E < E*
μ* = 525 MeV/GAUSS
f
r
R_s

Figure 9

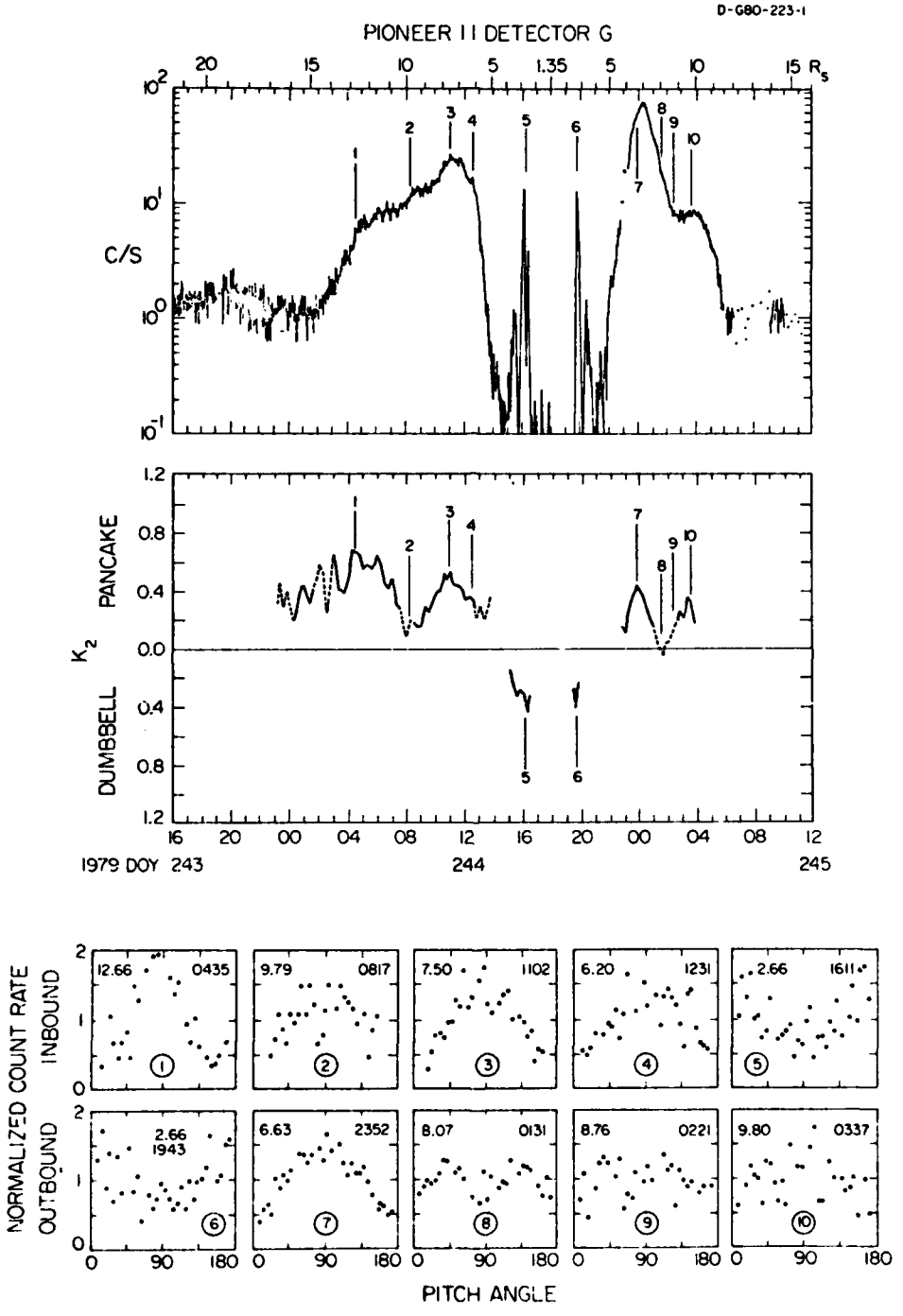
D-G80-223-1
PIONEER 11 DETECTOR G
20 15 10 5 1.35 5 10 15 R_S
10^2
10^1
10^0
10^{-1}
C/S
1 2 3 4 5 6 7 8 9 10
1.2 0.8 0.4 0.0 0.4 0.8 1.2
K_2
PANCAKE
DUMBBELL
1 2 3 4 5 6 7 8 9 10
16 20 00 04 08 12 16 20 00 04 08 12
1979 DOY 243 244 245
NORMALIZED COUNT RATE
INBOUND
OUTBOUND
12.66 0435 ①
9.79 0817 ②
7.50 1102 ③
6.20 1231 ④
2.66 1611 ⑤
2.66 1943 ⑥
6.63 2352 ⑦
8.07 0131 ⑧
8.76 0221 ⑨
9.80 0337 ⑩
0 90 180
PITCH ANGLE

Figure 10

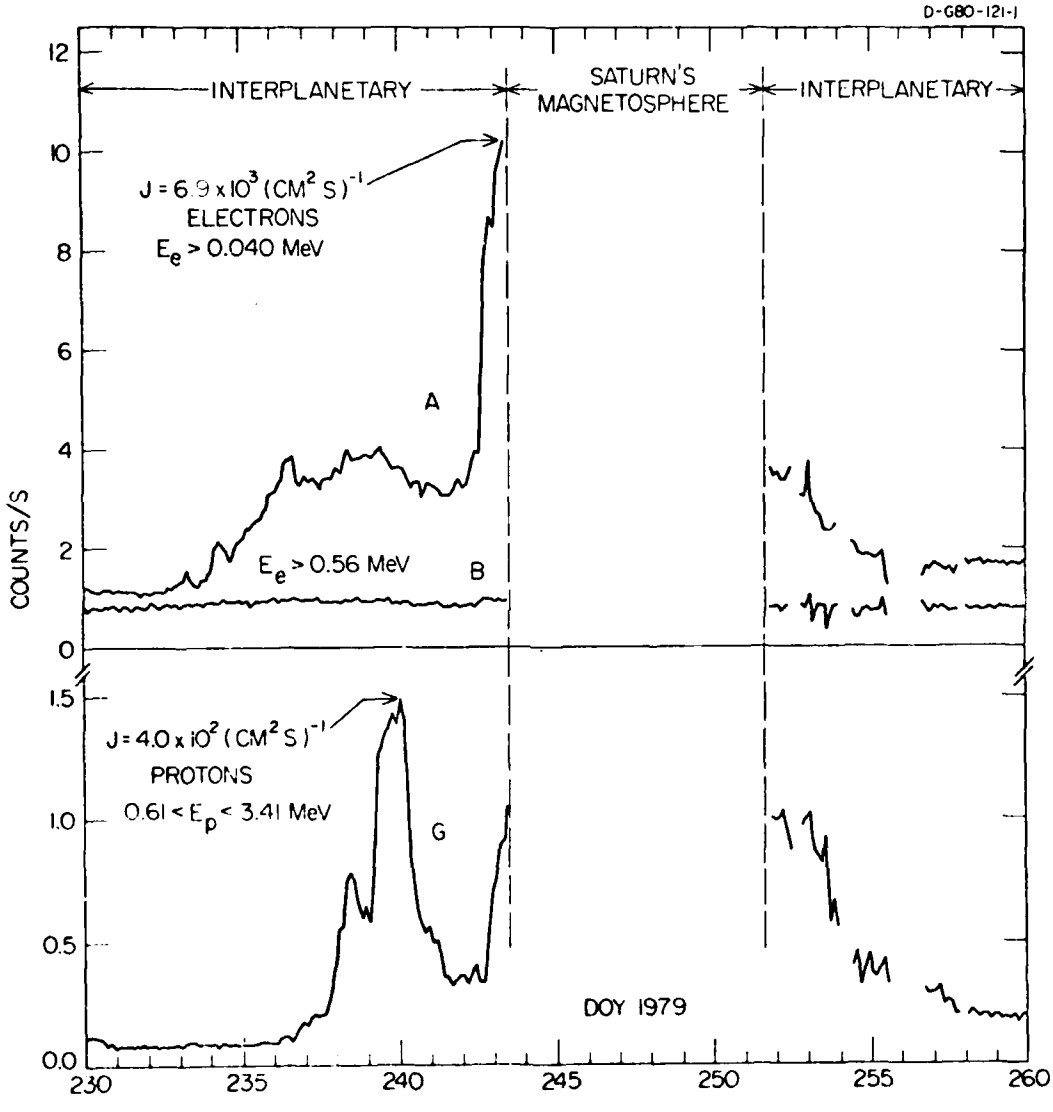
D-G80-121-1
INTERPLANETARY
SATURN'S MAGNETOSPHERE
INTERPLANETARY
J = 6.9 x 10³ (CM² S)⁻¹
ELECTRONS
Eₑ > 0.040 MeV
A
Eₑ > 0.56 MeV
B
COUNTS/S
J = 4.0 x 10² (CM² S)⁻¹
PROTONS
0.61 < Eₚ < 3.41 MeV
G
DOY 1979
0.0
0.5
1.0
1.5
0
2
4
6
8
10
12
230
235
240
245
250
255
260

Figure 11

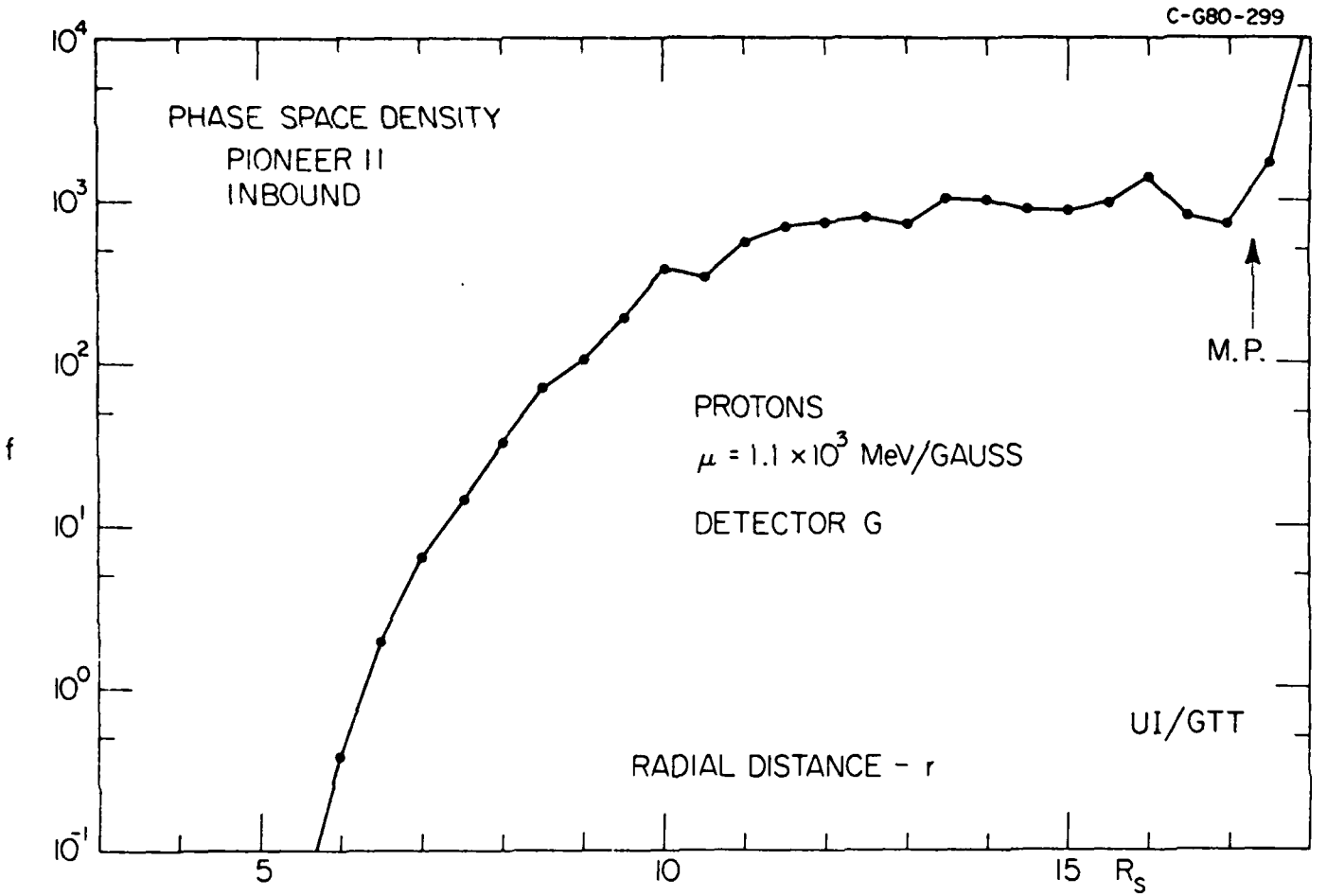
C-G80-299
PHASE SPACE DENSITY
PIONEER 11
INBOUND
M.P.
PROTONS
$\mu = 1.1 \times 10^3$ MeV/GAUSS
DETECTOR G
UI/GTT
RADIAL DISTANCE - r
f
10^4
10^3
10^2
10^1
10^0
10^{-1}
5
10
15 R_S

Figure 12

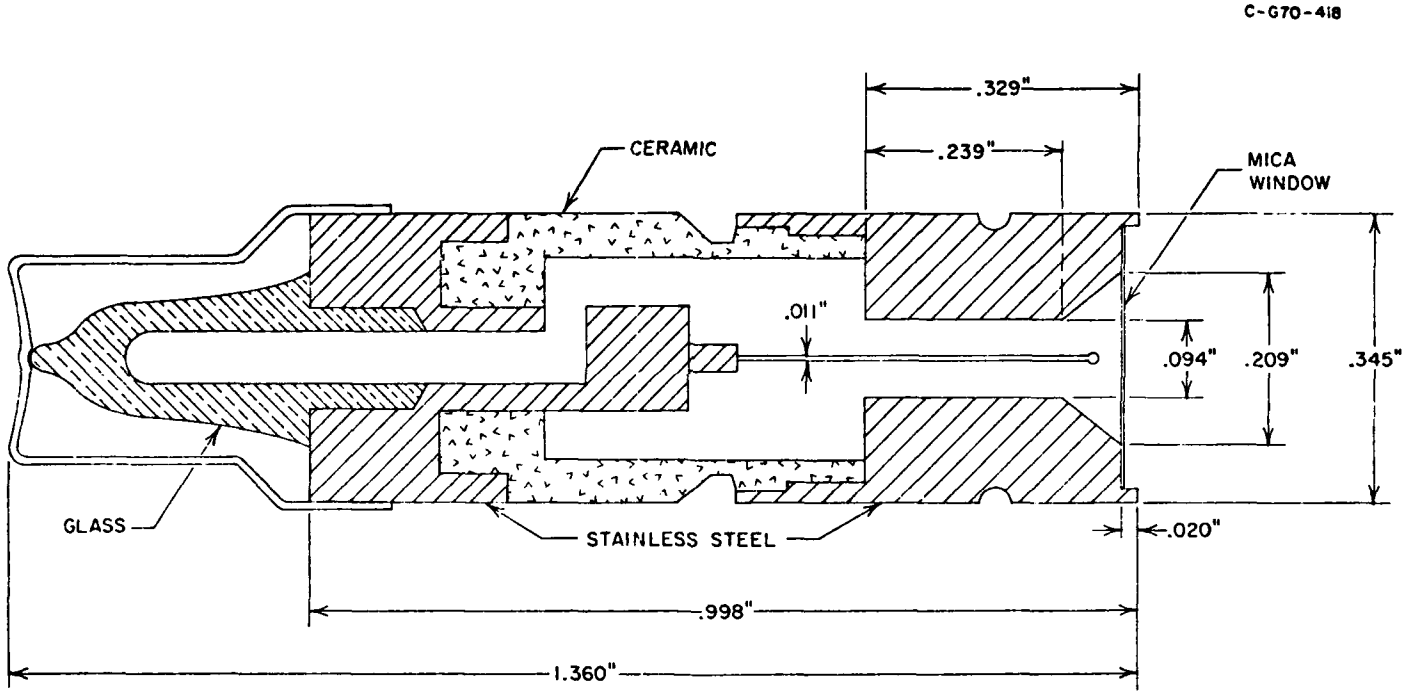

EON 6213

Figure 13

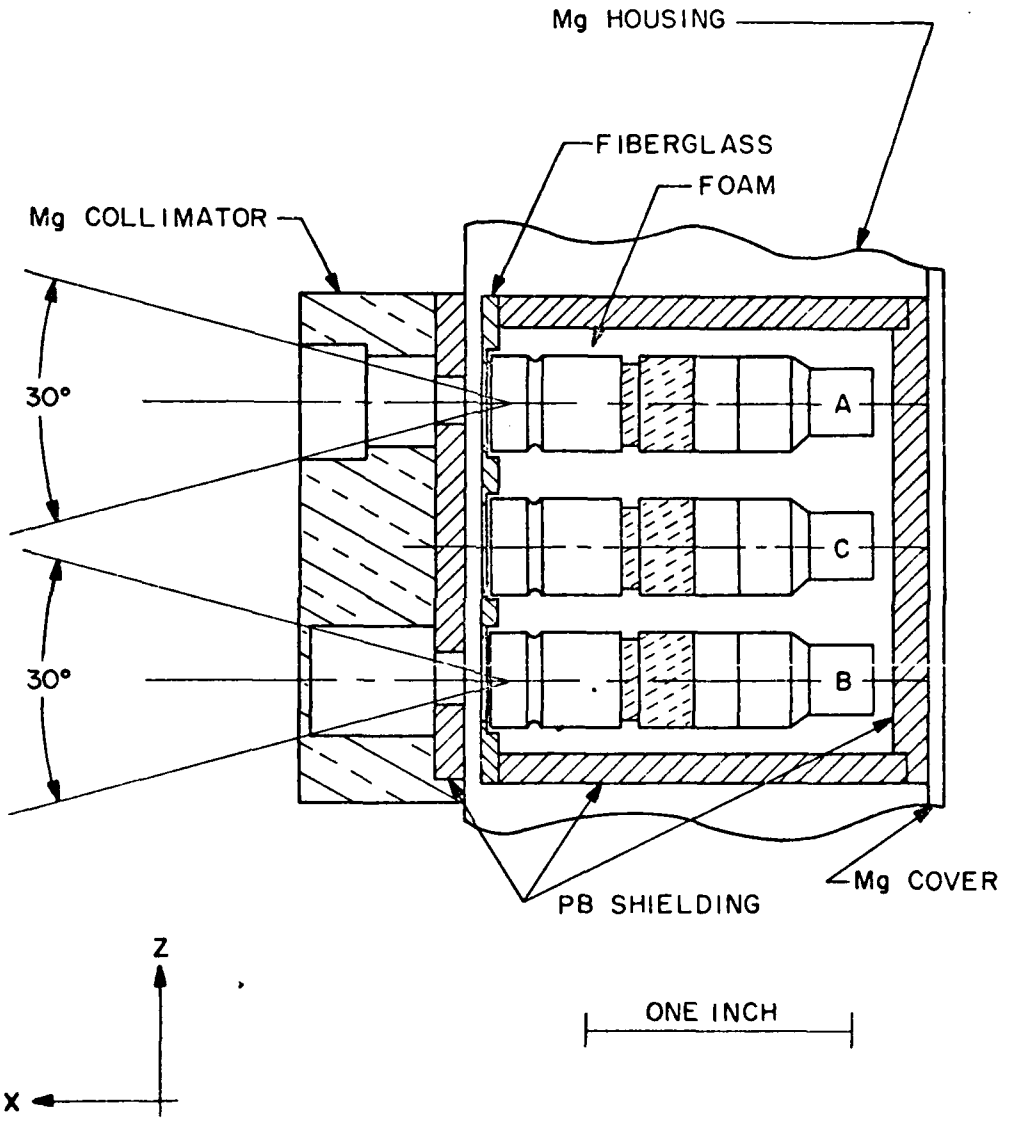

GEIGER-MUELLER TUBE TELESCOPE

Figure 14

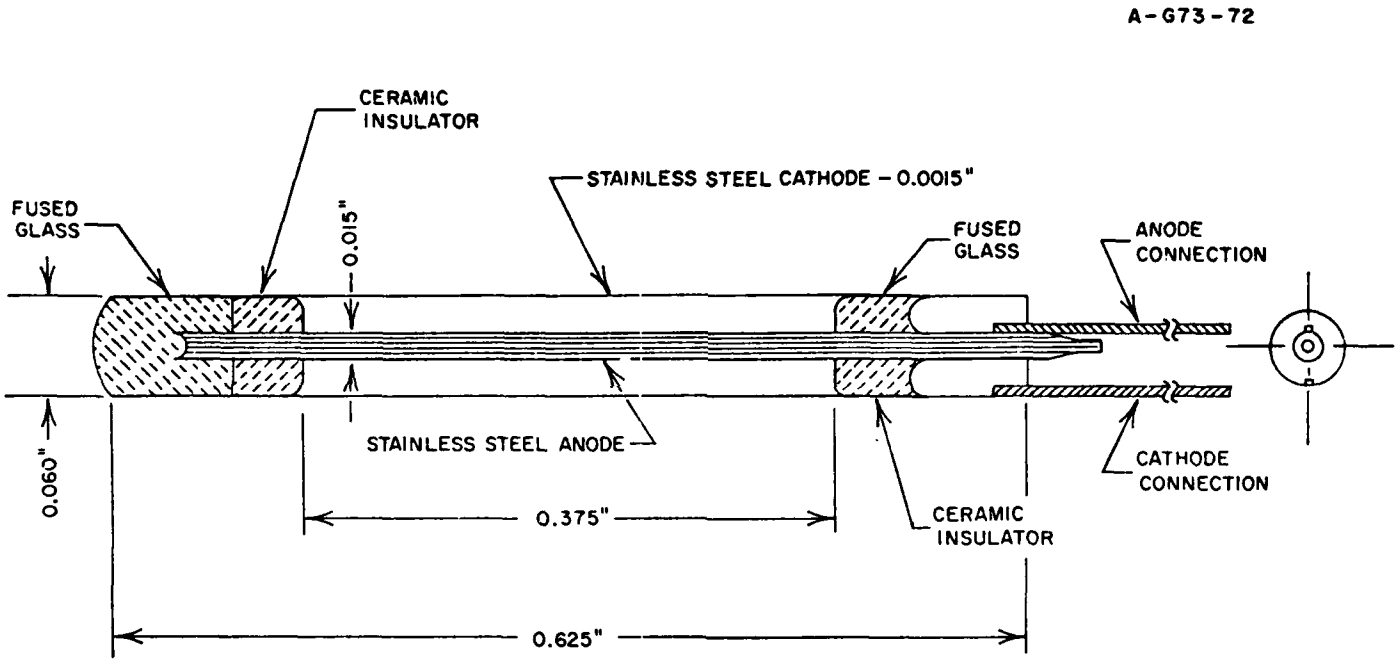

EON 5107

Figure 15

A-669-677

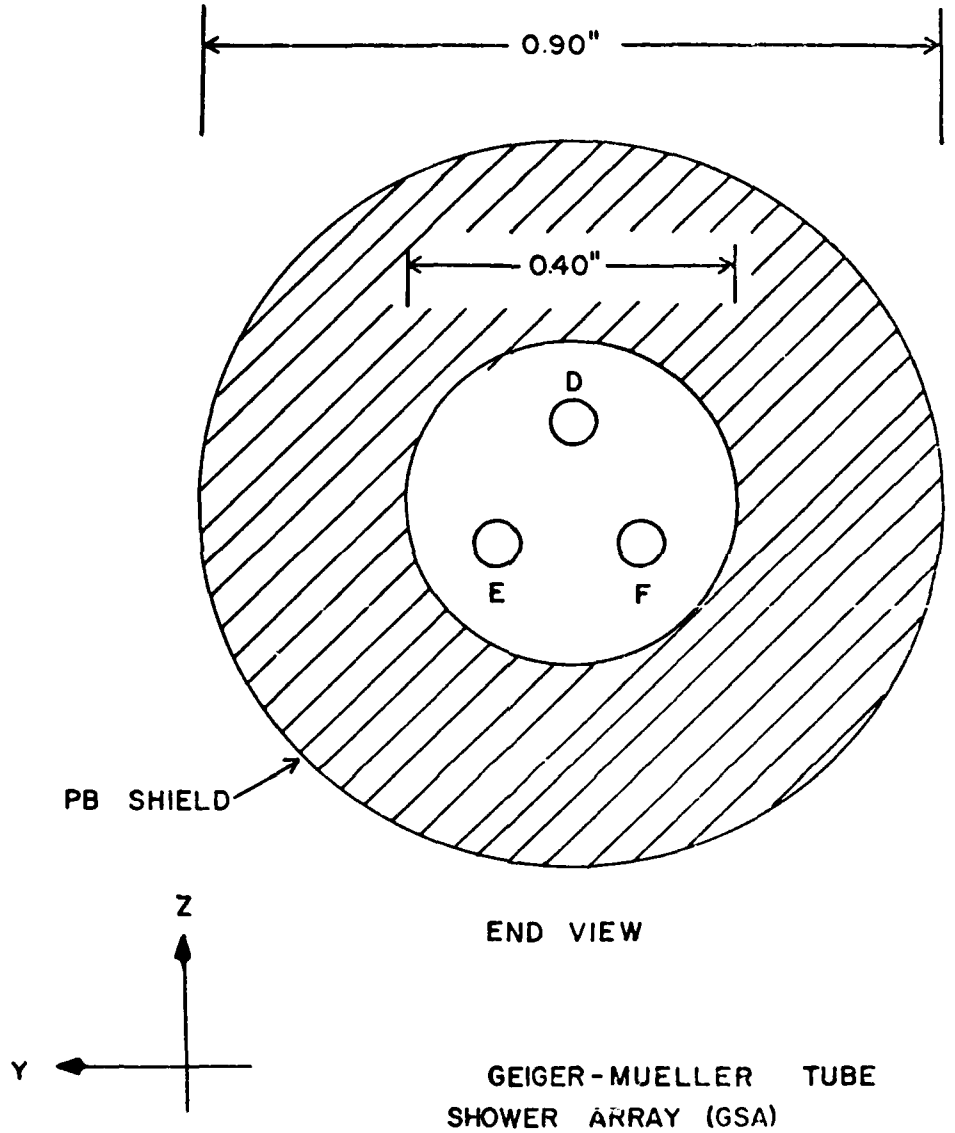

END VIEW

GEIGER-MUELLER TUBE
SHOWER ARRAY (GSA)

Figure 16

A-G73-12-2

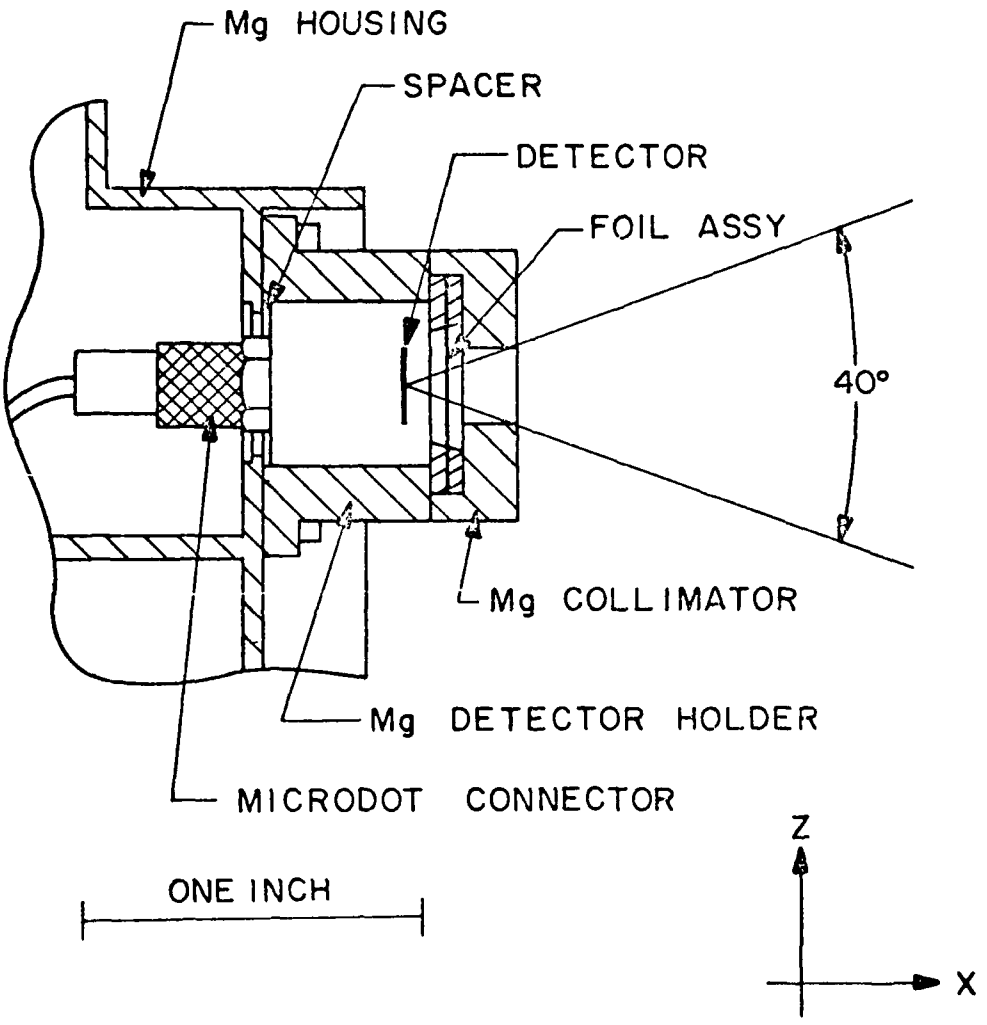

SOLID STATE DETECTOR

Figure 17

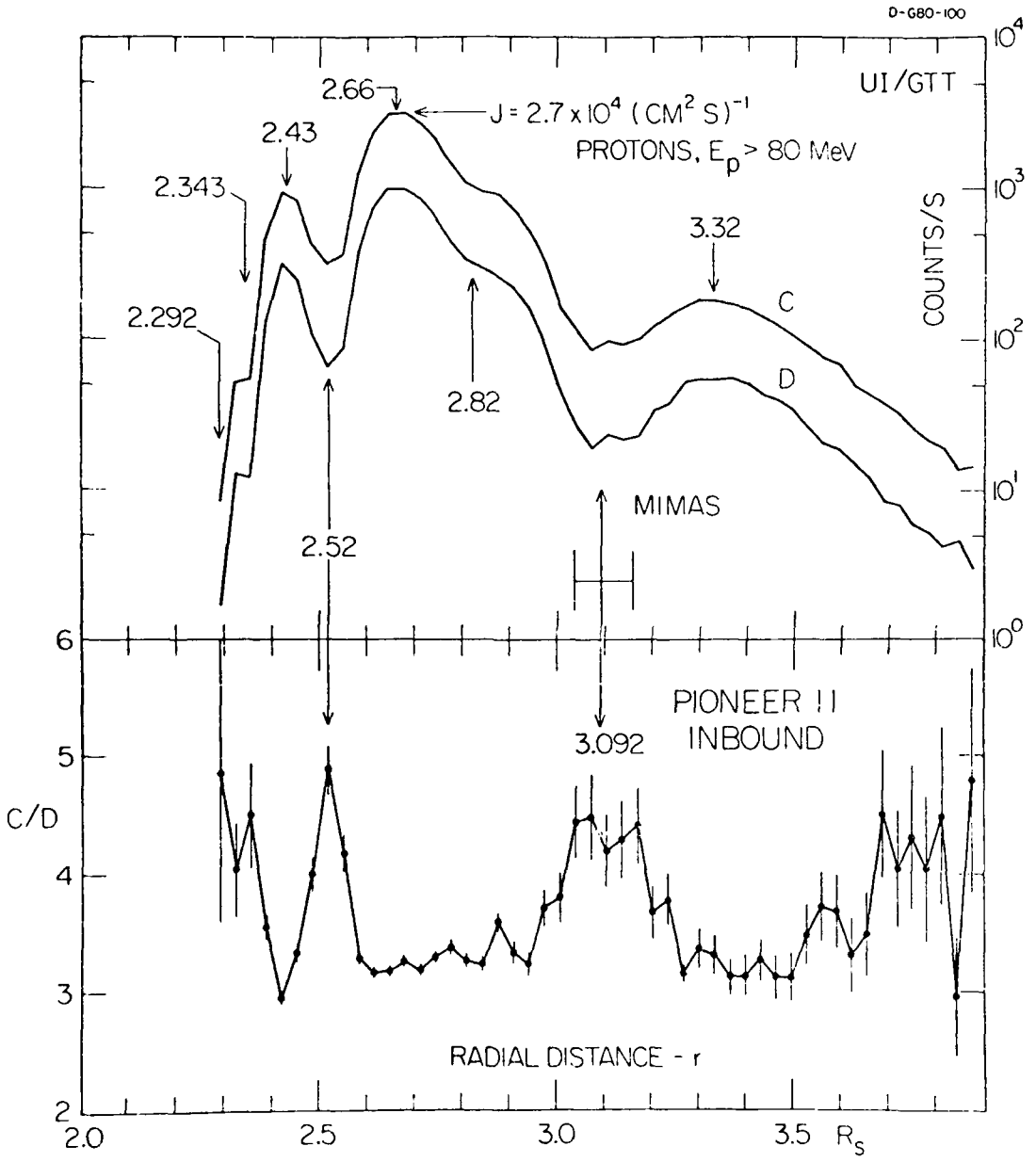
D-680-100
UI/GTT
2.66
J = 2.7 x 10^4 (CM^2 S)^-1
PROTONS, E_p > 80 MeV
2.43
2.343
2.292
3.32
C
D
2.82
2.52
MIMAS
COUNTS/S
10^4
10^3
10^2
10^1
10^0
6
5
4
3
2
C/D
PIONEER 11
INBOUND
3.092
RADIAL DISTANCE - r
2.0
2.5
3.0
3.5
R_S

Figure 18

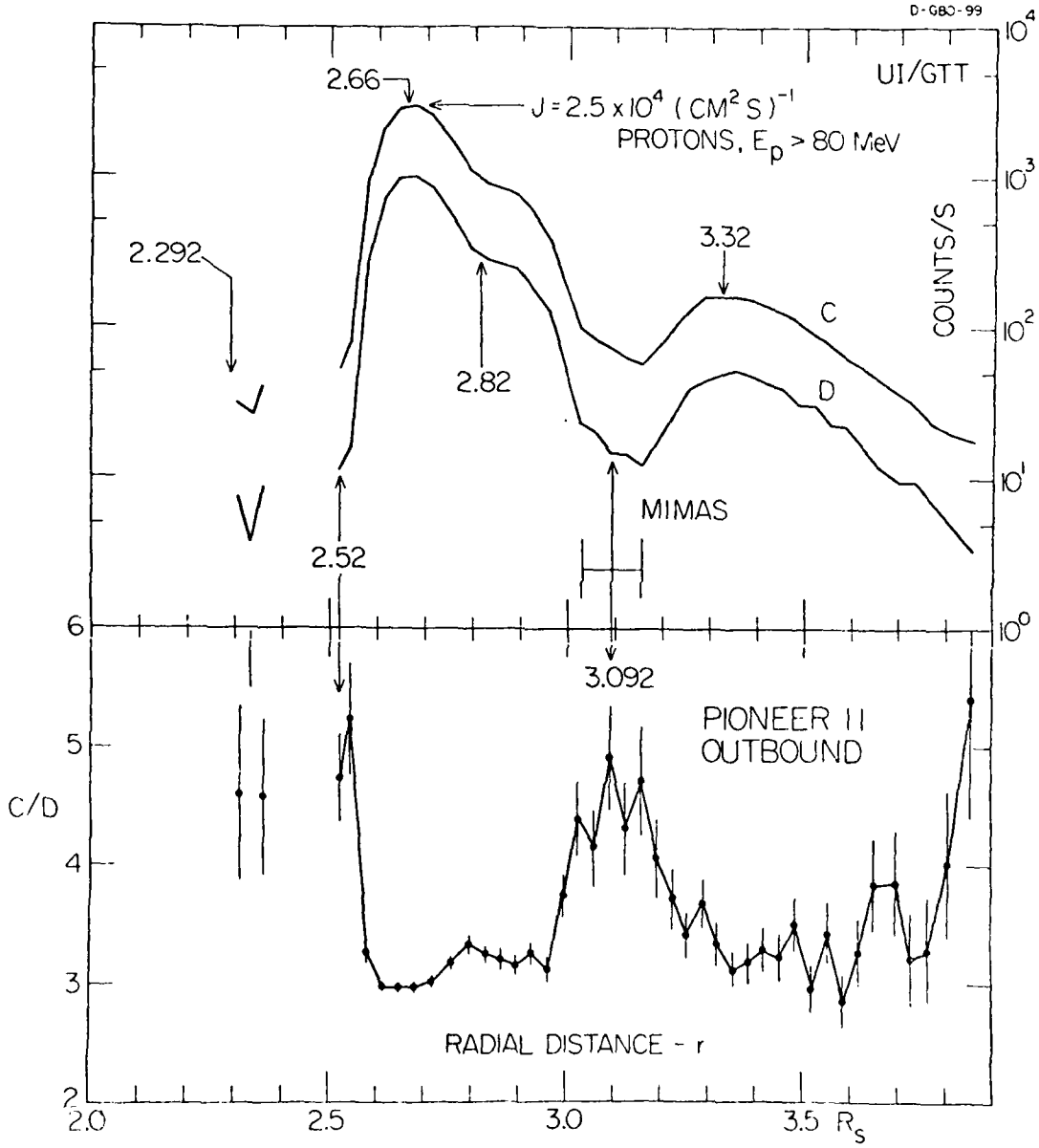
D-GBO-99
UI/GTT
2.66
J = 2.5 x 10^4 (CM^2 S)^-1
PROTONS, E_p > 80 MeV
2.292
3.32
C
2.82
D
COUNTS/S
MIMAS
2.52
3.092
PIONEER 11
OUTBOUND
C/D
RADIAL DISTANCE - r
2.0
2.5
3.0
3.5 R_S

Figure 19


DAT
FILM